Materials for life sciences

3D printed poly(lactic acid)-based nanocomposite scaffolds with bioactive coatings for tissue engineering applications

Maria-Eirini Grigora[1] , Zoi Terzopoulou[2,*] , Diana Baciu[3], Theodore Steriotis[3] , Georgia Charalambopoulou[3] , Eleni Gounari[4] , Dimitrios N. Bikiaris[2] , and Dimitrios Tzetzis[1,*]

[1] *Digital Manufacturing and Materials Characterization Laboratory, School of Science and Technology, International Hellenic University, 14km Thessaloniki, 57001 N Moudania, Greece*

[2] *Laboratory of Polymer and Colors Chemistry and Technology, Department of Chemistry, Aristotle University of Thessaloniki, 54124 Thessaloniki, Greece*

[3] *National Center for Scientific Research "Demokritos", 15341 Ag. Paraskevi Attikis, Greece*

[4] *Biohellenika Biotechnology Company, Leoforos Georgikis Scholis 65, 57001 Thessaloniki, Greece*

ABSTRACT

In this work, the effect of two different types of bioactive coatings on the properties of 3D printed poly(lactic acid)/montmorillonite (PLA/MMT) nanocomposite scaffolds was examined. To improve their suitability for bone tissue engineering applications, the PLA nanocomposite scaffolds were coated with (i) ordered mesoporous Strontium bioglass (SrBG) and (ii) SrBG and nanohydroxyapatite (nHA) using a simple dip coating procedure. The effect of the coatings on the morphology, chemical structure, wettability and nanomechanical properties of the scaffolds was examined. The hydrophilicity of PLA nanocomposite scaffolds increased after the SrBG coating and increased even more with the SrBG/nHA coating. Moreover, in the case of PLA/MMT/SrBG/nHA 3D printed scaffolds, the elastic modulus increased by $\sim 80\%$ and the hardness increased from 156.9 ± 6.4 to 293.6 ± 11.3 MPa in comparison with PLA. Finally, the in vitro biocompatibility and osteogenic potential were evaluated using bone marrow-derived stem cells. The coating process was found to be a fast, economical and effective way to improve the biomineralization and promote the differentiation of the stem cells toward osteoblasts, in comparison with the neat PLA and the PLA/MMT nanocomposite scaffold.

https://doi.org/10.1007/s10853-023-08149-4

GRAPHICAL ABSTRACT
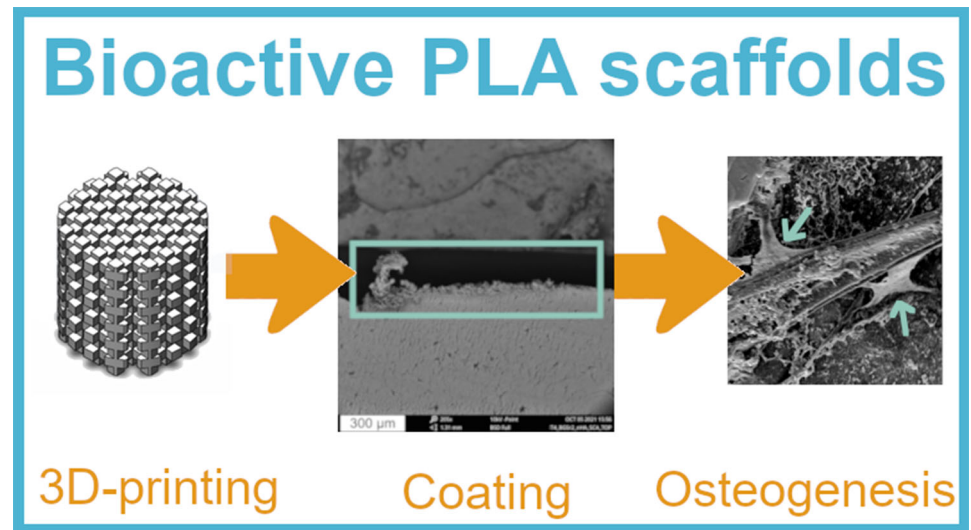
Introduction

Bone is a unique tissue that can repair damage after it occurs [1]. Natural bone is a composite material consisting of mineralized extracellular matrix (ECM) and cells which is complex and hierarchically structured [2]. To provide tissue repair and regeneration, a scaffold is utilized as a replacement for missing bone at the site of the defect, with or without bone-specific growth factors and (or) cells [3, 4]. The purpose of a scaffold is to create a 3D platform for cell and tissue growth [5]. 3D printing has been widely investigated as a promising strategy for fabrication of bone tissue engineering scaffolds [6–8]. Fused filament fabrication (FFF) is commonly used to fabricate scaffolds with material extrusion [9]. Furthermore, 3D printing offers an advantage in the design of complex geometries that successfully integrate with the host tissue [10]. FFF is one of the most common additive manufacturing technologies due to its simplicity and cost-effectiveness, and a plethora of material and design customizations [11].

PLA is gaining great attention in the field of biomedicine due to its biodegradability, biocompatibility, ecofriendly nature and good processability [12, 13]. Additionally, it can be 3D printed (3D

printability) with the potential to be used in a range of applications, including bone tissue engineering [14–17]. Porous PLA scaffolds have been found to be potential reconstruction matrices for damaged tissues and organs [18]. Preliminary clinical and radiographic evaluation has shown that PLA implants are secure, yield excellent functional outcomes as compared to metallic implants and give a quicker osteotomy bone healing [17]. However, the surface of PLA lacks cell attachment sites as it is quite hydrophobic and cannot promote osteoconductivity or osteoinductivity. To achieve the desirable mechanical properties, cell attachment and bioactivity, PLA nanocomposites with bioactive fillers such as bioceramics are a common choice [19]. PLA nanocomposites can be 3D printed using FFF technology [11]. A great number of studies report the use of thermoplastic polymers such as PLA along with ceramics to achieve desirable properties in manufacturing of biomedical 3D printed scaffolds via FFF [11]. Corcione et al. [20] prepared pellets of PLA-HA composite through premixing of hydroxyapatite [HA, $Ca_{10}(PO_4)_6(OH)_2$] powder with PLA pellets by utilizing a rotomoulding machine and used FFF technology to fabricate a PLA-HA composite filament. Yang et al. [21] used PLLA-modified HA (P-HA) nanoparticles blended with PLLA in order to

fabricate a composite material for bone tissue engineering.

Adding the bioceramics in the bulk polymer causes them to be entrapped, and most of the filler is not close to the surface of the produced filaments, so it cannot come in contact with cells and as a result, an excessive amount of filler is used. To overcome this, a bioactive ceramic coating can be applied on the scaffold [10, 22–25]. These coatings provide the scaffold with bioactivity and roughness that improves cell growth [26–28]. Some of the most common bioceramics used to coat scaffolds are bioglasses, tricalcium phosphate (β-TCP) and HA [9, 14, 15, 20, 29–35], due to their bioactivity and ability to enhance osteoinduction and osteoconduction, as well as their similarities to the mineral phase of natural bone tissues.

In this work, PLA-based scaffolds were fabricated with FFF for bone tissue engineering applications. To improve the mechanical properties of the scaffold, montmorillonite (MMT), a 2D nanophyllosilicate clay, was added during filament preparation in PLA. In our previous work, it was found that the optimum content of MMT was 4 wt.% [36]. MMT is much cheaper than bioceramics and readily available. It is also bioinert and improves the strength of polymer-based scaffolds while retaining their biocompatibility [37–40].

To functionalize the surface of the scaffolds, post-fabrication dip coating was employed (a) using a strontium-containing ordered mesoporous bioglass (SrBG) alone and (b) combining SrBG with nanosized HA (nHA). SrBG was chosen because the substitution of CaO by SrO in the composition of typical calcium phosphosilicate bioglasses such as Bioglass® has emerged as a promising route for developing new, efficient materials that can substantially contribute to the bone's regeneration and osteogenic differentiation processes [41]. Apart from the well-known beneficial effect of long-term Sr-based treatment on improving osteoporosis patients' bone mineral density for decreasing fracture risk, several studies have reported that the presence of Sr^{2+}, which is chemically similar to Ca^{2+}, can significantly alter the mechanism of biological activity and boost the performance of different kinds of bioglasses. It has been demonstrated that Sr^{2+} could remarkably improve cementogenic gene expression, osteoid formation, collagen synthesis and alkaline phosphatase (ALP) activity, while controlling calcium metabolism and promoting bone formation as well as osteoblast cell proliferation also by inhibiting osteoclast activity and bone resorption [2, 42]. In our previous work [43], we demonstrated that when the CaO component (10% molar ratio) in a SiO_2-CaO-P_2O_5 mesoporous bioglass was fully replaced by Sr, the resulting SiO_2-SrO-P_2O_5 system (containing Sr at a 10% molar ratio) showed augmented bioactivity over its CaO counterpart. Herewith, we focused on investigating the potential beneficial effect of increasing the bioglass Sr content up to 15% molar ratio, in a way to attain enhanced bioactivity.

While bioglasses are excellent in bonding to bones and stimulating new bone formation, nHA is highly bioactive, interacts rapidly with proteins and facilitates the healing of hard tissues. In fact, the beneficial properties of bioglasses and HA are complementary, as bioglasses lead to weaker cell adhesion than HA, but they are better in imparting osteoinduction [44]. Additionally, the combination of ions of bioglasses (Si) with Sr and nHA was found to have a synergistic effect on promoting bone regeneration [45]. Coating the scaffolds with the bioceramics instead of adding them in the filaments ensures their presence on the surface and allows them to interact with the cells while reducing the quantity of bioceramics needed, thus decreasing the overall cost of the scaffold.

Four groups of porous scaffolds were prepared using FFF and post-fabrication dip coating, namely PLA, PLA/MMT, PLA/MMT/SrBG and PLA/MMT/SrBG/nHA. The printability of the scaffolds was examined using a stereoscope. Moreover, the effect of two different bioactive coatings on the physicochemical and biological properties of 3D printed PLA/MMT scaffolds was then evaluated. To do so, a wide range of techniques, such as infrared spectroscopy (IR), X-ray diffraction (XRD), differential scanning calorimetry (DSC), thermogravimetric analysis (TGA) and water contact angle (WCA) measurements, were employed. Furthermore, the mechanical properties were examined with nanoindentation testing. Finally, the effect of the scaffolds on in vitro bioactivity, viability of bone marrow mesenchymal stromal cells (BM-MSCs) and osteogenic differentiation using an osteogenesis differentiation kit was examined.

Materials and methods

Materials

Poly(lactic acid) (PLA) under the trade name of PLA-Ingeo™ Biopolymer 3052D of Natureworks was generously offered by Plastika Kritis S.A. (Iraklion, Greece). Joncryl ADR® 4400 was supplied by BASF (Ludwigshafen, Germany) with epoxy equivalent weight of 485 g/mol and its weight–average molecular weight is 7100 g/mol. Cloisite® 20A (MMT) was supplied by Southern Clay products (Gonzales, TX, USA); it is a montmorillonite-based organoclay, modified with dimethyl, dehydrogenated tallow quaternary ammonium and it has interlayer distance of 26 Å. Hydroxyapatite nanoparticles (nHA) with diameter 20–50 nm in a 5–10% (w/v) aqueous colloidal dispersion were purchased from Alfa Aesar ThermoFisher (Kandel, Germany). Polyethylene glycol (PEG) particles (average Mn 10.000 g/mol), tetraethyl orthosilicate (TEOS) (reagent grade 98%), triethyl phosphate (TEP) (purum 99.8 + %), strontium nitrate $Sr(NO_3)_2$ (ACS reagent, $\geq$ 99%), cetyltrimethylammonium bromide (labeled as CTAB) and ethanol were purchased from Sigma-Aldrich Chemical Company. Sodium hydrate pellets were supplied from Mallinckrodt Company. Moreover, NaCl, KCl, $K_2HPO_4 \cdot 3H_2O$, $MgCl_2 6H_2O$, Ca $(NO_3)_2 \cdot 4H_2O)$, $CaCl_2$, Na_2SO_4 reagents, tris(hydroxymethyl) aminomethane $(HOCH_2)_3CNH_2$ and HCl used for preparing SBF solution were also purchased from Sigma-Aldrich Chemical Company. All other reagents and chemicals were purchased from Sigma-Aldrich and were of reagent grade.

Synthesis of mesoporous ternary bioglasses

Ordered mesoporous bioactive glasses based on ternary (SiO_2-SrO-P_2O_5) systems were synthesized through a hydrothermal method previously described [46], following, however, slightly modified protocol, by using polyethylene glycol and cetyltrimethylammonium bromide, as nonionic co-surfactant and cationic surfactant, respectively. Briefly, for the preparation of the ternary bioglass with 75% SiO_2, 15% SrO and 10% P_2O_5 molar ratio (hereafter denoted as SrBG), proper amounts of PEG and sodium hydrate were dissolved in distilled H_2O under vigorous stirring, followed by the addition of CTAB. After stirring for 1 h at room temperature,

$Sr(NO_3)_2$, tetraethyl orthosilicate and triethyl phosphate were added. The mixture was kept under vigorous stirring at room temperature for 24 h and then transferred into 120 mL Teflon-lined autoclaves. The autoclaves were sealed and heated at 80 °C for 48 h and then allowed to naturally cool down to room temperature. The products were collected by filtration and washed several times with distilled H_2O and ethanol and dried at 100 °C overnight. Finally, the white powder obtained was calcined in air at 600 °C for 5 h with a heating rate of 9 °C/min.

Preparation of materials for filament fabrication

The PLA/MMT nanocomposite filament was fabricated using PLA with 2 wt.% Joncryl and 4 wt.%MMT according to our previous work [36]. The addition of 4 wt.% MMT improves the printability of PLA filaments and the surface quality of 3D printed specimens, as well as the mechanical behavior at compression testing [36]. PLA/MMT nanocomposite filament was produced using FFF technology. Briefly, the powder mixture of the selected materials (PLA, Joncryl, MMT) was placed into the hopper of a 3Devo desktop Filament Maker-Composer 350 (3Devo, Utrecht, the Netherlands), and the PLA/MMT nanocomposite filament was extruded into 1.75-mm-diameter filament with temperatures ranging from 170 °C to 210 °C, setting from feeding zone to the nozzle. The filament fabrication process lasted for 4 h. The deviation of the filament thickness was 5 μm. No post-printing processing was required.

Design and manufacturing of scaffolds

Different types of scaffolds were designed using computer-aided design software SolidWorks 2020 and then were tested though FFF technology to achieve the best 3D printing performance. The criteria of this evaluation were the pores dimensions as well as the 3D printing accuracy and quality of 3D printed specimens. Cylindrical scaffolds with open porosity were designed with different interconnection. After preliminary tests with different squared pores with sizes from 500 × 500 μm up to 1000 × 1000 μm, the best 3D printing quality and accuracy results were achieved with 1000 μm pore size. According to the literature, the range of pore diameters suitable for bone tissue engineering is

between 300 μm to 1000 μm [47–49]. Therefore, larger pores are preferred for cell proliferation and growth compared to smaller ones, as they will occlude later during the progressive growth, leaving room accessible for oxygen and nutrient supply as well as promoting further vascularization in developing bone tissues [50]. Open porosity (51.6%) cylindrical scaffolds (diameter = 13 mm, height = 13 mm) with 1000 × 1000 μm squared pores were designed using SolidWorks 2020. The scaffolds were fabricated using PLA/MMT filament containing 2 wt.% Joncryl and 4 wt.% MMT by utilizing a XYZ da Vinci SUPER 3D printer with an extrusion nozzle of diameter D = 400 μm and a tempered glass building plate set at 60 °C. This temperature was used in order to achieve better stability of the 3D printed specimen during the printing process and create a closed first layer for better cell culture performance. Figure 1 shows the design of the porous scaffold (top view and isometric view). The reason for choosing custom design of scaffolds was to increase the surface area on the top of the scaffolds for further increase in the cell proliferation. For the physicochemical characterization and nanoindentation testing, non-porous 3D printed specimens were also produced (100% infill), similar to the designs of our previous study [51]. No features of the 3D CAD design were smaller than the resolution limit of the FFF-printer of 0.4 mm. A neat PLA scaffold was also produced for comparison.

Post-fabrication scaffold coating

The dip coating protocol was a combination of the process described by Chen et al. [52] and Mondal et al. [32]. Prior to coating, alkali surface treatment was used in order to activate the surface of the specimens [52]. The 3D printed specimens were immersed in a 0.5 M aqueous ammonia solution (pH = 11.5) under magnetic stirring (185 rpm) at room temperature for 4 h. Afterward, they were dried at 55 °C for 30 min. Two different types of coatings were deposited on the PLA/MMT 3D printed specimens. To coat the scaffolds with SrBG, the scaffolds were immersed in a 2 wt.% aqueous SrBG dispersion (prepared by magnetic stirring and ultrasonication) under magnetic stirring at 185 rpm for 1 h at 70 °C followed by ultrasonication at 70 °C for 10 min and finally more magnetic stirring at 185 rpm for 20 min at 70 °C. To coat the scaffolds with both SrBG and nHA, after the SrBG coating, a consecutive dipping in the nHA dispersion (after diluting the supplied nHA dispersion 1.5 times) took place using the same protocol. All the specimens were dried at 75 °C for 10 min. After cooling at room temperature, the coated samples of PLA/MMT/SrBG and PLA/MMT/SrBG/nHA were further ultrasonicated for 3 min, while they were immersed in 100% ethanol at room temperature to remove any unbound residual SrBG and/or nHA. The different types of scaffolds are prepared, and their abbreviations are shown in Table 1.

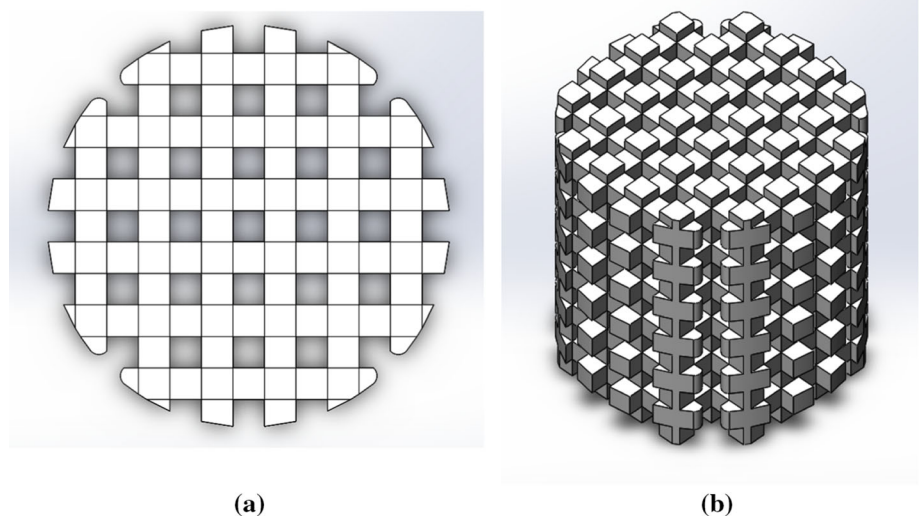**Figure 1** Design of the scaffold **a** top view, **b** isometric view.

(a)   (b)

Table 1 List of the scaffolds, their composition and their abbreviations

Name	PLA content (wt.%)	Joncryl content (wt.%)	MMT content (wt.%)	Coating
PLA	98	2	–	–
PLA/MMT	94	2	4	–
PLA/MMT/SrBG	94	2	4	SrBG
PLA/MMT/SrBG/nHA	94	2	4	SrBG, nHA

Characterization

Characterization of mesoporous ternary bioglasses

The powder X-ray diffraction (PXRD) patterns of the SrBG bioglass samples were recorded on a Rigaku R-AXIS IV imaging plate detector mounted on a Rigaku RU-H3R rotating copper anode X-ray generator ($\lambda = 1.54$ Å). SEM images of the developed materials were obtained using a JEOL, JSM 7401F field emission (JEOL Ltd., Tokyo, Japan) microscope equipped with a Gentle Beam mode. SEM images of the developed materials were obtained using a JEOL, JSM 7401F field emission (JEOL Ltd., Tokyo, Japan) microscope equipped with a Gentle Beam mode. The accelerating voltage was 2 kV, and the magnification is 5000 times.

The pore properties of SrBG were determined by nitrogen adsorption/desorption measurements at 77 K using a volumetric gas adsorption analyzer (AUTOSORB-1-MP, Quantachrome Instruments). Prior to measurement, the sample was appropriately outgassed (at 250 °C for 12 h) under high vacuum (10^{-6} mbar), while ultrapure N_2 was used. The Brunauer–Emmett–Teller (BET) area of the sample was calculated, following the BET consistency criteria. Pore size distributions were deduced by fitting the adsorption isotherms based on a non-local density functional theory (NLDFT) kernel developed for N2 at 77 K on silica materials with cylindrical pores.

The biological activity of the bioglass samples was assessed in vitro by monitoring the formation of an apatite layer on the surface of SrBG particles that were immersed in a stimulated body fluid (SBF) solution prepared according to Kokubo's method [53]. First, the samples were soaked in the SBF solution (1.5 mg mL^{-1}) at 37 °C and pH = 7.4 for 1, 3, 7 and 14 days, respectively. The bottles were placed inside a Shaking Incubator (LSI-3016R, Labtech) at a fixed temperature of 37 °C, and a speed of 200 rpm was used. At each selected time point, the particles were removed from the SBF solution by centrifugation at 5000 rpm for 5 min, rinsed with acetone to cease further reaction, air-dried at room temperature and analyzed using XRD to detect the HA phase formation.

Physicochemical characterization of the scaffolds

The morphology of the surface of the scaffolds was observed with optical microscopy (stereoscope) and scanning electron microscopy (SEM). Photographs were captured using a Jenoptik (Jena, Germany) ProgRes GRYPHAX Altair camera attached to a ZEISS (Oberkochen, Germany) SteREO Discovery V20 microscope and the Gryphax image capturing software. Pore size dimensions were measured from 10 randomly selected pores based on stereoscope images (taken at 7.5 × magnification). The diameters were reported as mean ± standard error of the mean. For SEM (Phenom ProX, ThermoFisher Scientific, Waltham, MA, USA), a small porous scaffold from each sample was 3D printed for examining the coating. Specimens were mounted onto double adhesive conductive carbon tabs (TED Pella, Redding, CA, USA) on an aluminum stub (placed in a charge reduction holder), with gold coating to increase electrical conductivity and scanned at an accelerating voltage of 15 kV. The samples, prior to SEM analysis, were coated with gold using a sputter coater (SC 7620 model, Quorum Technologies, East Sussex, UK) for 90 s, 18 mA, and observed by SEM with an accelerating voltage of 15 kV. Energy-dispersive X-ray spectroscopy (EDX) was also used to analyze the elemental composition of the surface of the specimens; elemental mapping was used to verify the successful and uniform distribution of coating in the surface of scaffolds. The accelerating voltage applied was 15 kV and the magnification was 2000 times.

Infrared (IR) spectra were recorded with a Cary 670, Agilent Technologies, equipped with a diamond attenuated total reflectance accessory, ATR, model GladiATR, Pike Technologies. The spectra were collected in the range 4000–400 cm^{-1} at a resolution 4 cm^{-1} with 32 scans.

Thermogravimetric analysis (TGA) was carried out employing a SETARAM SETSYS TG–DTA 16/18 instrument (Setaram instrumentation, Lyon, France). A suitable sample quantity (2 ± 0.2 mg) was placed in an alumina crucible while an empty alumina crucible was used as reference. After that, the samples were heated from room temperature to 600 °C in a 50 mL min^{-1} flow of N_2 at a heating rate of 20 °C min^{-1}.

Water contact angle was measured on 3D printed specimens, including non-porous and porous scaffolds. The apparent contact angle of water was studied using a water contact angle tester (Ossila Contact Angle Goniometer L2004A1) in order to measure the surface wettability of nanocomposites with and without coating. The sessile drop method was used to analyze the WCA of the samples. 25 μL of distilled water was added dropwise on the top surface of 3D printed plates (n = 3), as well as on the top surface of scaffolds. Images were captured within 20 s with a high-resolution camera and processed using the Ossila Contact Angle Software.

Mechanical properties through nanoindentation testing

The nanomechanical properties of PLA/MMT/SrBG and PLA/MMT/SrBG/nHA were investigated using the nanoindentation technique and were compared to PLA and PLA/MMT4 without coating according to our previous research [36]. A dynamic ultramicro-hardness tester DUH-211 (Shimadzu Co., Kyoto, Japan) using a 100-nm-radius triangular pyramid indenter tip (Berkovich-type indenter) was used to determine the mechanical performance of PLA/MMT4 nanocomposites with two types of coating. During indentation test, a controlled load (P) with a peak load of 3 mN was applied through a diamond tip on the surface of solid 3D printed specimens. This peak load was held for 3 s, and the indentation depth was recorded as a function of load. Subsequently, the indenter was unloaded, to a load of zero. The maximum indentation load was applied to the indenter during the creep time. The modulus and hardness

were obtained as the average value of ten measurements.

In vitro biomineralization of the scaffolds

For the biomineralization assessment, the scaffolds were incubated in simulated body fluid (SBF), which was prepared according to Kokubo and Takadama [53]. Scaffolds with cylindrical shape 15 × 2 mm (diameter x height) were soaked in 20 mL of SBF for 14 days at 37 °C. After two weeks, the scaffolds were washed gently with distilled water, dried for 1 h under vacuum and characterized by SEM–EDX using the conditions described previously.

Cell studies

Cultivation and genetic modification of Bone Marrow Mesenchymal Stromal Cells (BM-MSCs)

To perform the experiments, Biohellenika SA provided BM-MSCs isolated as previously described [54]. In brief, bone marrow was diluted in RPMI 1640 medium (GIBCO), mixed gently with 7 mg collagenase (Sigma-Aldrich) and incubated shaking, for 45 min, at RT. After filtration, the suspension layered over Ficoll (Histopaque) solution and centrifuged. The mononuclear cell layer was collected carefully in DMEM (BIOWEST) supplemented with 10% FBS (BIOWEST) and 1% pen-strep (SIGMA) while 2*10^5 cells/cm^2 were plated into T75 flasks, maintained in a humidified atmosphere at 37 °C with 5% CO_2 for cultivation. Between the 2 and 3 passages, a Pt2-Venus-neo-mediated nucleofection was performed as described from our previous studies [55, 56]. More precisely, 3*10^5 cells were mixed with 10 μg of plasmid DNA SB100X transposaseandpT2-Venus-neo transposon expression plasmids (1:5 ratio) and were put to electroporation according to the manufacturer's instructions (Lonza). The cells were then plated in one well of a 6-well plate in the presence of DMEM full medium until reaching a 90% confluency, whereas 100 mg/mL G418 was added for the selection of the genetically modified BM-MSCs for further culture.

Preparation of the materials and cells' seeding

All the materials were sterilized in gradually reduced ethanol concentrations (100%–70%–50%) and after

being washed three times with ddH$_2$O were let to overnight air-dry under sterile conditions in 12-well plates. BM-MSCs were detached from plastic surfaces using Trypsin–EDTA 1 × in PBS (BIOWEST) and were counted in a Neubauer cell counting chamber. 4*10^5 cells were re-suspended in DMEM full medium and were subsequently placed above the materials of each condition in 200 μL final volume using 16G needle to penetrate porous materials. Upon air-drying for 4 h in the incubator, 2 mL DMEM full medium was added per well for the culture initiation.

Observation under fluorescence microscope

The observation of the cells above the materials was performed, 24 h after cellular attachment, under a fluorescence HBO 50 mercury lamp as well as reflectors with fluorescence filter (excitation 488 nm, emission 509 nm), while the Fluorescence Lite software module of AxioVision LE (Carl Zeiss) was used for downloading and editing the photos.

3-[4,5-Dimethylthiazole-2-yl]-2,5-diphenyltetrazolium bromide (MTT) assay

In order to assess the cytotoxicity levels of materials, the MTT assay was performed (SIGMA) 24 and 72 h after the initial cell plating. Briefly, after the medium removal from the wells, MTT reactant was introduced in a ratio of 1:10 in DMEM culture medium and was followed by a 4-h incubation in 37 °C with 5% CO$_2$. Upon the removal of the MTT, 1 mL/well of DMSO was introduced for one additional hour of incubation in the same conditions. The plastic PS surface of the cell plates was used as control. The reduction in the MTT was counted at wavelengths 570 and 630 nm (PerkinElmer).

Osteogenic differentiation—Alizarin red staining and cpc quantification

The induction of differentiation toward osteocytes was performed using a StemPro osteogenesis differentiation kit (GIBCO) for 28 days with medium changes every 3–4 days. BM-MSCs, plated in plastic surfaces in the same number as the rest of the other groups, untreated or induced to differentiate, were used as negative or positive control group, respectively. The successful induction of differentiation toward bone cells was verified with Alizarin Red

staining. The quantification of the procedure was carried out with 10% cetylpyridinium chloride (CPC) in 10 nM sodium phosphate, pH 7.0 for 15 min at room temperature. The extracts were 10 times dissolved in 10% CPC, and the Alizarin Red concentration was counted at 562 nm in a PerkinElmer spectrometer.

Scanning electron microscopy (SEM)

After 48 h of cellular attachment on the materials and after the completion of osteogenesis induced cultivation, all the materials were fixed in 4% paraformaldehyde for 20 min at room temperature and were subsequently let to air-dry overnight. A detailed investigation of the scaffolds surface was observed using a scanning electron microscope (Phenom ProX, ThermoFisher Scientific, Waltham, MA, USA). The samples were first covered with gold. 3D printed scaffolds were characterized with operation at an accelerating voltage of 10 kV0. The images were acquired from the top view of the scaffold to investigate the cell culture for each type of specimens. Samples were mounted onto double adhesive conductive carbon tabs (TED Pella, Redding, CA, USA) on an aluminum stub (placed in a charge reduction holder) without coating and scanned at an accelerating voltage of 10 kV.

Statistical analysis

Unless otherwise stated, one-way ANOVA with post hoc Tukey test was used. The software used was GraphPad Prism 6. A p-value of < 0.05 was considered statistically significant.

Results and discussion

Characterization of SrBG

The SEM image of the SrBG sample Figure S1a shows that calcination at 600 °C leads to the formation of aggregated nanoparticles with a diameter between 90–270 nm. The pore properties of the SrBG sample were determined by N$_2$ adsorption/desorption measurements at 77 K. Figure S1b shows the obtained isotherm, which, according to the classification of International Union of Pure and Applied Chemistry (IUPAC), is of Type IV. In fact, the

isotherm has the characteristics of the completely reversible Type IV(b), which is typical for (usually ordered) mesopores having widths smaller than 4 nm. Additionally, at higher relative pressures the isotherm appears as a Type IV(a) case, with a pronounced H3/4 hysteresis loop, implying that larger mesopores (> 4 nm) are also present. The size of these pores extends even to the macropore region as revealed by the lack of an adsorption plateau and the exponential increase in the adsorbed quantity at relative pressures close to unity. Actually, these (disordered) pores are formed between the SrBG primary particles (see SEM image of Figure S1a). The SrBG was found to have a BET area of 255 m^2/g and, according to NLDFT analysis, a pore volume of 0.15 cm^3/g for pores smaller than 10 nm. In addition, NLDFT fitting revealed a very narrow distribution of pore diameters centered at around 3.5 nm (Figure S1c).

The mesoporous structure of the SrBG sample was also confirmed by XRD analysis. Indeed, in the low angle region, the XRD pattern of SrBG (Figure S1d) shows Bragg peaks/shoulders at $2\theta \approx 2.4$, 4.2 and 4.9°, revealing an ordered hexagonal network of mesopores (space group p6mm, d_{10} = 3.65 nm, lattice parameter a_0 = 4.2 nm) [63–67]. On the other hand, the wide-angle XRD pattern of the calcined Sr-containing bioglass depicted in Figure S1e points to orthorhombic symmetry (Space Group: Pmcn) and is mainly related to the strontium carbonate ($SrCO_3$) strontianite phase [57, 58] as observed upon comparing the powder profile with the expected peak positions (PDF No: 5–418).

XRD measurements were also used to assess the in vitro bioactivity of the SrBG material, after soaking a certain quantity in SBF solution, for a prolonged period (up to 14 days). XRD diffractograms were recorded at different time points (before and after 1, 3, 7 and 14 days of immersion in SBF) in order to confirm the formation of crystalline hydroxyapatite (Figure S1f). It can be seen that the characteristic apatite peak in the range of 31.5–31.8°, corresponding to (211) reflection planes, occurs after soaking in SBF for 3 days [57–63]; in contrast, the $SrCO_3$ peaks are suppressed, implying that the respective crystals disappear during this period. The hydroxyapatite peaks became more pronounced from the third day of immersion onwards, showing that the formation of the hydroxyapatite was enhanced upon increasing the time of exposure to SBF. In addition, new peaks of increasing intensity were observed, e.g., at around 28° and 46° that can be associated with the (210) and (312) crystalline planes of strontium apatite, respectively. On this basis, the peak in the range of 31.5–31.8° can be associated with the overlapping of the (211) plane of hydroxyapatite and the (300) plane of strontium apatite, as also reported before [58].

Preparation and characterization of 3D printed scaffolds

Morphology

A macroscopic photograph of the 3D printed scaffolds is shown in Fig. 2. The details and the overall quality of the scaffolds containing MMT is better in
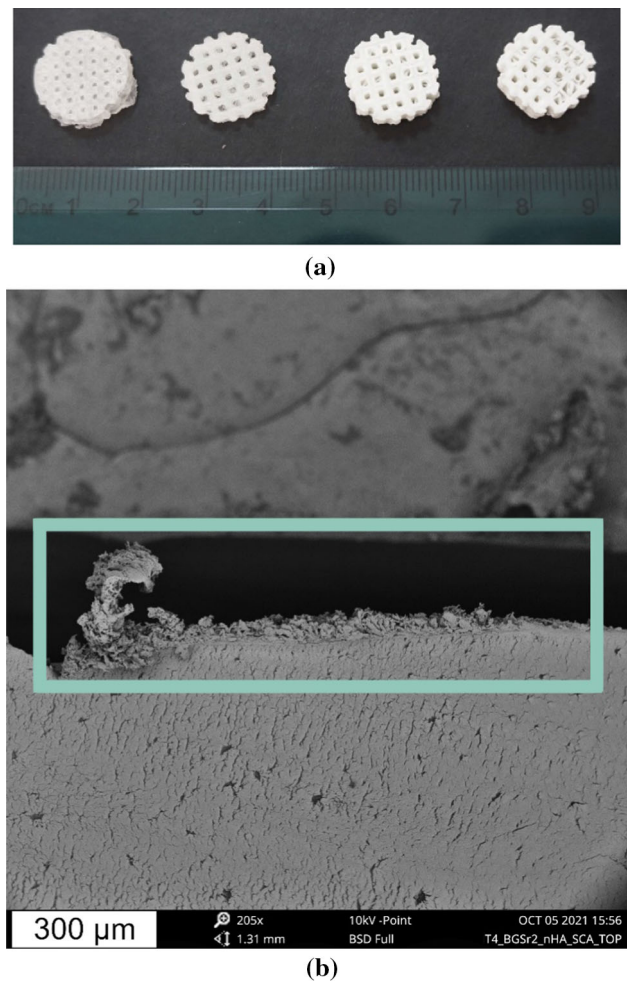

(a)

(b)

Figure 2 a Photographs of 3D printed cylinder scaffolds from left to right PLA, PLA/MMT, PLA/MMT/SrBG, PLA/MMT/SrBG/nHA, **b** SEM image of PLA/MMT/SrBG/nHA showing the coating in the boxed area.

comparison with neat PLA, as MMT can improve its printability [36]. The morphology and microstructure of PLA nanocomposite scaffolds were observed using a stereoscope. Representative stereoscope images of the 3D printed scaffolds are shown in Fig. 3. In comparison with PLA, the PLA/MMT scaffolds have larger pores, closer to the theoretical dimension, as well as better printability, demonstrated by the better uniformity of the pores. According to our previous study [36], MMT enhances the mechanical properties of the scaffold, and this can ensure the stability of the structure in bone tissue engineering applications. Furthermore, MMT improved the printability of the PLA scaffolds, ensuring better structural accuracy and control of the size of the pores of the scaffolds, which is a crucial parameter in tissue engineering. After coating with SrBG and nHA, the surface of the

scaffolds appears smoother, opaque and less shiny, indications that a coating layer thick enough to cover the surface of PLA exists. The perceived smoothness could be due to the bioceramics covering the defects and spaces between the struts, but without compromising the porosity.

The porosity of scaffolds is crucial for tissue engineering applications, while it affects cell growth and enhances cell proliferation. For bone tissue engineering, microporosity is considered necessary to allow cell proliferation and biomineralization. Open porosity is also crucial as it enables the flow of culture medium, blood and oxygen, as well as tissue growth [64]. The range of pore diameter suitable for bone tissue engineering is from 300 μm up to 1000 μm [49]. The average pore dimension of the scaffolds is reported in Table 2.

Figure 3 Stereoscope images of the scaffolds (top view) **a** PLA, **b** PLA/MMT, **c** PLA/MMT/SrBG and **d** PLA/MMT/SrBG/nHA.
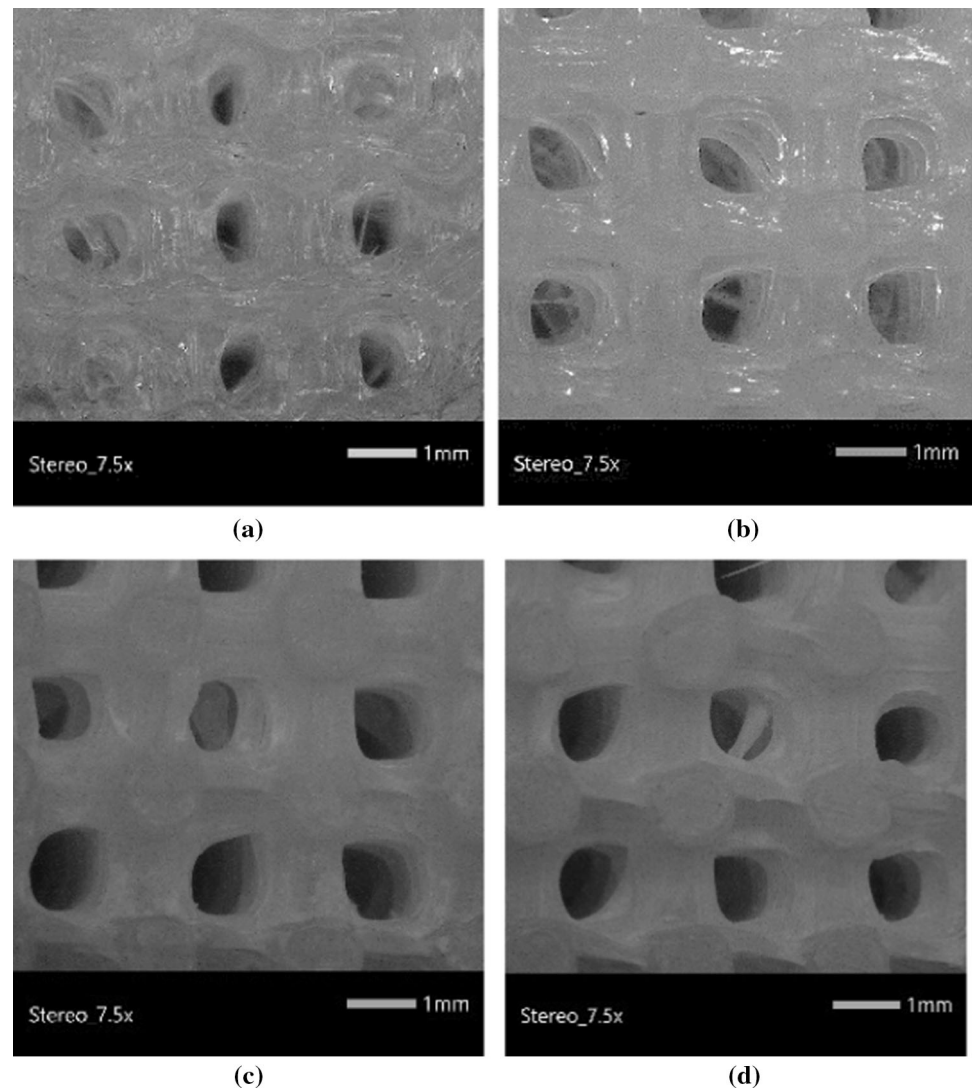
Table 2 Pore dimensions of PLA/MMT scaffolds

Sample	Average pore dimension (μm)
PLA	712.99 ± 74.52
PLA/MMT	995.67 ± 24.31****
PLA/MMT/SrBG	994.95 ± 9.81****
PLA/MMT/SrBG/nHA	994.80 ± 8.62****

**** $p < 0.0001$ in comparison with PLA

SEM images of the cross section of the scaffolds are presented in the left column of Figure S2. While PLA (Figure S2a) and PLA/MMT (Figure S2b) have smooth and clean surfaces, both PLA/MMT/SrBG and PLA/MMT/SrBG/nHA (Figure S2c and Figure S2d) have a thin layer of coating visible in the highlighted areas. The SrBG coating is $\sim$ 25 μm and the SrBG/nHA coating is $\sim$ 60 μm. Chen et al. achieved a $\sim$ 1 μm coating of nHA on PLA scaffolds [52]. The increased thickness of the coating in this work can be attributed to the differences in the experimental procedure, namely increased concentration of the bioceramics (>1 wt.%) and, dipping temperature 70 °C instead of room temperature, accompanied by sonication for 10 min. Thus, the combination of alkali pretreatment and mild heating during dipping increased the density and the thickness of the coatings. In the PLA/MMT/SrBG/nHA scaffold, some peeling of the coating has occurred because of the cutting of the specimens with a microtome. Upon closer examination of the scaffolds' surfaces, both coatings are formed by clusters of individual particles (Fig. 4e and g) ranging from a few micrometers down to submicron sizes, making the surface rough and irregular. With the additional layer of nHA, the coating becomes denser. The roughness of the surfaces of the PLA/MMT/SrBG/nHA and the PLA/MMT/SrBG causes the light to diffuse, so these two scaffolds appear matte (Fig. 3). To confirm that the observed particles are SrBG and nHA, EDX analysis was performed. The Si, Sr and P elements of SrBG were detected (Figure S3e), and the intensity of Ca and P increased after the second coating with nHA (Figure S3g).

Choosing post-printing coating with bioactive particles over their direct incorporation in the filaments helps overcome some important problems. Oftentimes, when preparing thermoplastic composite filaments with bioglass or HA, the composites are prepared beforehand using the solution mixing approach using organic solvents to ensure good filler dispersion [56, 65, 66], since the hydrophilic ceramics are incompatible with hydrophobic polymers. Additionally, adding a sufficient quantity of fillers in order to get enough particles on the surface of the filaments and obtaining the desired hydrophilicity can deteriorate printing quality [67, 68]. With the coating approach, only water is used as a solvent and all the bioactive particles are located on the surface of the scaffolds, while when adding them in the filament only a handful of surface particles can be detected [69–71].

Physicochemical characterization

The chemical structure of the coated scaffolds was examined by ATR spectroscopy. Figure 5 shows the ATR spectra of the scaffolds in the range of 4000–500 cm^{-1}. The spectrum of PLA shows small absorption bands in the range of 3700–3500 cm^{-1} assigned to O–H bending, at $\sim$ 2900 cm^{-1} of C–H stretching, at 1749 cm^{-1} caused by the C $=$ O stretching of polyesters, at 1456 cm^{-1} of –CH$_3$ asymmetric bending and C–O–C stretching at 1183 cm^{-1}, 1136 cm^{-1} and 1084 cm^{-1}. The bending vibrations of the C–H bending of the CH–OH end group appear at 1044 cm^{-1}. In the coated scaffolds, PLA/MMT/SrBG and PLA/MMT/SrBG/nHA, a broad peak can be noticed at around 3500–3000 cm^{-1} which indicates the presence of moisture, due to the hydrophilic nature of the coatings. The main ATR bands of PLA are retained in all the composite scaffolds, but the relative intensity of the C–H stretching and the C $=$ O stretching absorption bands is decreased. ATR is a surface technique; therefore, the presence of the coatings reduced the contribution of the bond vibrations of PLA to the final spectra. After careful examination of the region at 1200–600 cm^{-1}, small new peaks can be noticed, as well as the shift of the peak at 1044 cm^{-1}. In both PLA/MMT/SrBG and PLA/MMT/SrBG/nHA, a small band at 860 cm^{-1} can be attributed to the Si–O–Si bonds of the SrBG. The scaffold PLA/MMT/SrBG/nHA has an additional absorption band at 563 cm^{-1} which is a result of the P–O vibrations of the PO$_4^{3-}$ group of nHA. Finally, the shift of the hydroxyl band at 1044 cm^{-1} to smaller wave numbers is evidence of hydrogen bonding, which could take place between the

Figure 4 SEM images of the PLA-based scaffolds before (left column) and after (right) incubation in SBF for 14 days **a–b** PLA, **c–d** PLA/MMT, **e–f** PLA/MMT/SrBG and **g–h** PLA/MMT/SrBG/nHA scaffolds.
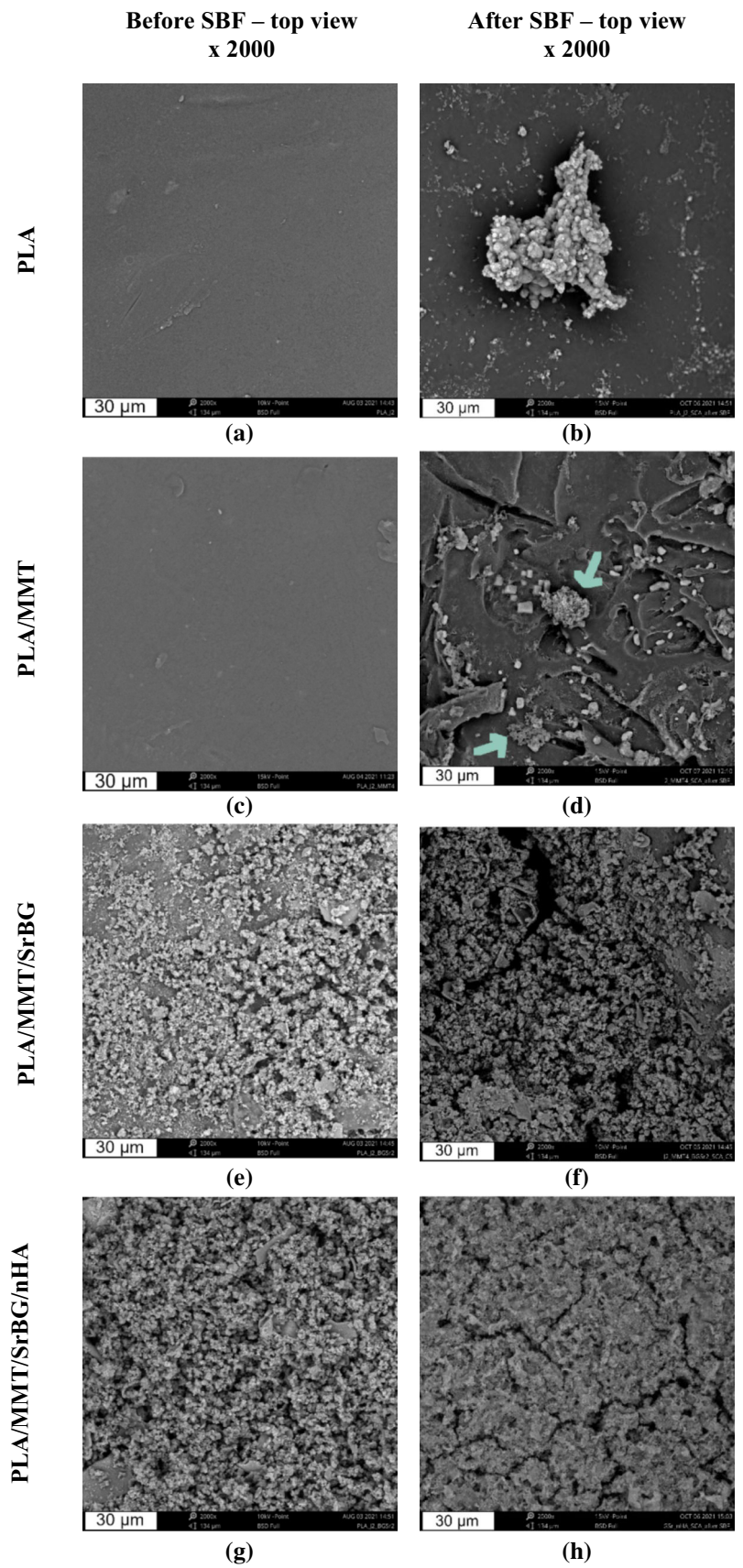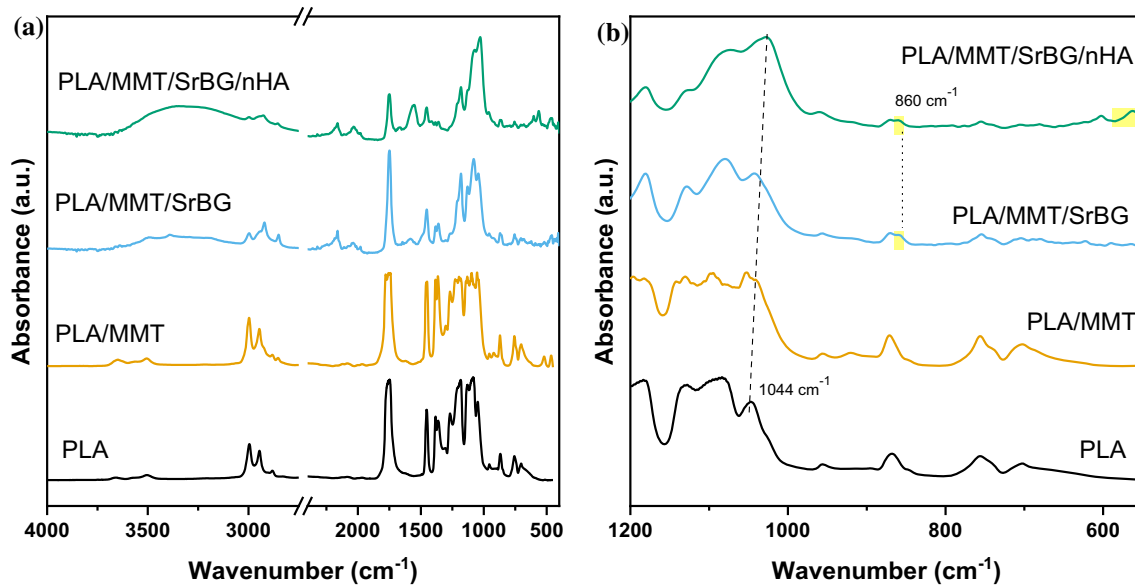
Figure 5 ATR spectra of PLA, PLA/MMT, PLA/MMT/SrBG and PLA/MMT/SrBG/nHA scaffolds **a** in the wave number range $4000 - 500$ cm^{-1} and **b** zoom-in the region 1200–600 cm^{-1}.

hydroxyls of PLA and the oxygens of the end groups of both SrBG and nHA.

Thermal stability of PLA/MMT/SrBG and PLA/MMT/SrBG/nHA was assessed using thermogravimetric analysis (TGA). The mass loss and DTG curves of PLA, PLA/MMT and the coated PLA/MMT nanocomposites are shown in Figure S4 and the thermal degradation characteristics in Table 3. PLA is a polyester with excellent thermal stability, since it does not begin to degrade until T_o = 359.6 °C. The addition of bioglasses in polyesters dramatically deteriorates their thermal stability [56, 72], because they can catalyzethe degradation reactions [73]. In

this work, the coatings do not have an important effect on the thermal stability, as the T_o, $T_{d,10\%}$ and T_p values of the PLA/MMT/SrBG and PLA/MMT/SrBG/nHA scaffolds remain almost unchanged in comparison with PLA neat and are reduced be a few degrees when compared with PLA/MMT. The small reduction can be attributed to the presence of moisture in the hydrophilic coatings. Thus, the method of coating the scaffolds with bioactive inorganics instead of adding them in the bulk of PLA is beneficial for its thermal stability. Being only on the surface of the scaffolds, the interface of SrBG and nHA with PLA is smaller and the extent of catalysis of the degradation reactions is much smaller.

Wettability

Hydrophilicity is crucial for adhesion and cell proliferation on the surface of PLA/MMT-coated specimens. The effect of two different coatings on the hydrophilicity was evaluated by measuring the WCA. The obtained mean WCA values are summarized in Fig. 6. According to our previous study [36], PLA had a contact angle of $60.47 \pm 2.82°$ and the addition of 4 wt.% MMT in the PLA matrix increased the contact angle to $62.51 \pm 8.51°$. This small increase in the hydrophobicity is a result of the modifier of the MMT used, which is hydrogenated tallow that
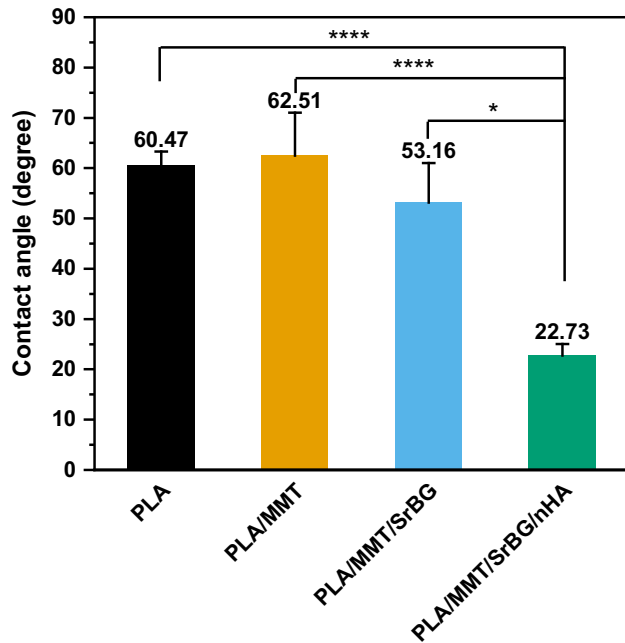
Table 3 Thermal degradation characteristics the PLA-based scaffolds

Sample	T_o (°C)	$T_{d,10\%}$ (°C)	T_p (°C)
PLA	359.6	352.3	380.5
PLA/MMT	364.7	349.4	380.8
PLA/MMT/SrBG	357.8	350.5	381.7
PLA/MMT/SrBG/nHA	358.7	348.4	380.6

T_o: extrapolated onset of degradation (the point of intersection of the starting mass baseline and the tangent to the TGA curve at the point of maximum gradient), $T_{d,10\%}$: temperature that corresponds to 10% mass loss, T_p: peak temperature of DTG where degradation occurs with the fastest rate

Figure 6 Mean water contact angle values for PLA, PLA/MMT, PLA/MMT/SrBG and PLA/MMT/SrBG/nHA 3D printed solid specimens. Bonferroni post hoc,*p 0.01–0.05;**p 0.001–0.01;***p 0.0001–0.001;****$p < 0.0001$.

reaching the lowest value of 22.73 ± 2.32° [75], which is expected to be beneficial for cell adhesion and infiltration of body fluids. In agreement with this work, nHA coatings have been reported to increase the hydrophilicity of 3D printed PLA scaffolds significantly [52]. Both SrBG and nHA increased the hydrophilicity of PLA because of their chemical structure, i.e., the abundant polar hydroxyl groups that facilitate water absorption [75]. Generally, the use of scaffolds in tissue engineering can be affected by surface wettability, since it improves cell attachment, migration and proliferation [76][76]. The effect of nHA and SrBG indicated that the combined coating greatly increased ($p < 0.0001$ compared to untreated PLA) the wettability of the PLA surface.

Mechanical and thermomechanical properties

Mechanical properties through nanoindentation testing

The nanomechanical properties of PLA/MMT/SrBG and PLA/MMT/SrBG/nHA nanocomposites were investigated on coated 3D printed specimens with nanoindentation testing. In order to calculate the values of hardness and elastic modulus, Oliver–Pharr [77] and previous research [78–81] were used. In Fig. 7a, the comparative load–depth curves are illustrated for PLA/MMT/SrBG and PLA/MMT/SrBG/nHA 3D printed specimens as measured from the nanoindentation tests and compared with PLA and PLA/MMT, reported in our previous work [36].
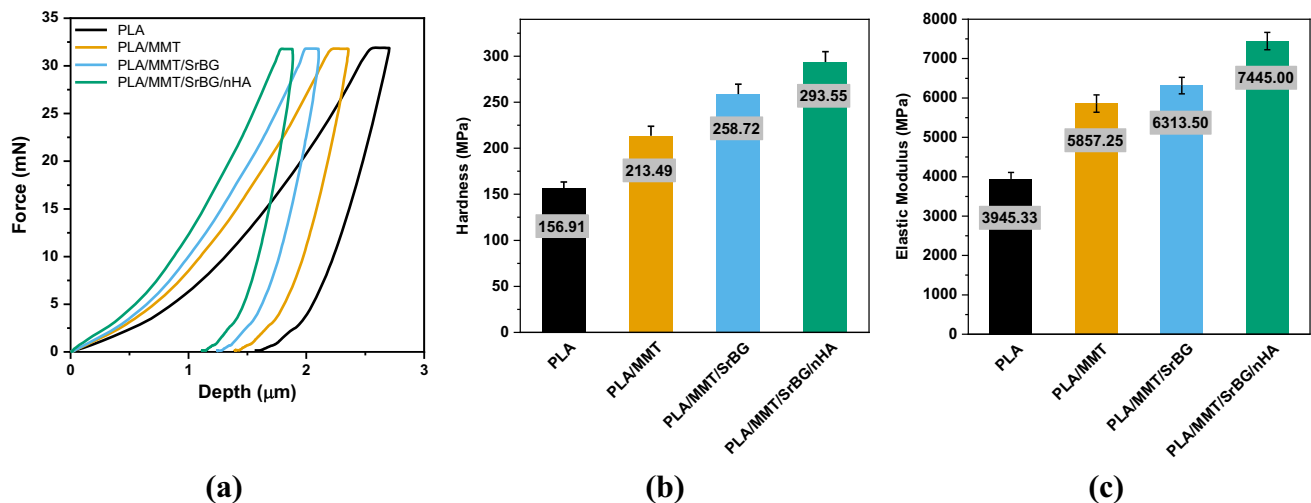
contains long aliphatic chains. This increase prevents the practical application of PLA/MMT tissue engineering scaffolds, as strong hydrophobic surfaces prevent cell attachment and migration [74]. The SrBG coating led to a decrease in the WCA of the scaffold's surface to 53.16 ± 7.85°. Moreover, the SrBG/nHA coating resulted in a further decrease in the WCA,

Figure 7 **a** Load–depth nanoindentation curves, **b** mean hardness and **c** mean elastic moduli values of PLA, PLA/MMT, PLA/MMT/SrBG and PLA/MMT/SrBG/nHA.

Table 4 Elastic moduli and hardness values from nanoindentation testing of PLA, PLA/MMT, PLA/MMT/SrBG and PLA/MMT/SrBG/nHA

Sample	Hardness (MPa)	E_i nanoindentation (N/mm^2)
PLA	156.91 ± 6.43	3945.33 ± 134.74
PLA/MMT	213.49 ± 10.36	5857.25 ± 222.11
PLA/MMT/SrBG	258.72 ± 10.92	6313.50 ± 208.54
PLA/MMT/SrBG/nHA	293.55 ± 11.31	7445.00 ± 219.06

Moreover, the present of MMT in PLA 3D printed scaffolds increased the strength of polymer scaffolds. According to Fig. 7a, it can be noticed that the representative load–depth curves shifted to the left with the coating of the specimens, resulting in higher stiffness. The range of the nanoindentation depth of PLA/MMT/SrBG was 1.98 to 2.09 μm and 1.76 to 1.88 μm for PLA/MMT/SrBG/nHA. Based on the equation of Oliver–Pharr [77], in the state of maximum controlled load, the sample with the lower nanoindentation depth exhibits the higher value of hardness.

The effect of the coatings on the nanomechanical properties of PLA/MMT scaffolds as measured from nanoindentation is summarized in Fig. 7b and c. The hardness of the coated specimens increased in comparison with both PLA and PLA/MMT. Compared to PLA, PLA/MMT/SrBG and PLA/MMT/SrBG/nHA showed an increase of 65% and 87%, respectively. Additionally, the elastic modulus of PLA/MMT/SrBG was calculated to be approximately 6314 MPa, reaching an increase of 60% compared to PLA. In the case of PLA/MMT/SrBG/nHA, the elastic modulus was measured to be 7445 MPa, which is an 80% increase in comparison with PLA. When adding bioglass directly in PLA filaments, the elastic modulus remained the same or decreased with higher bioglass contents (> 1 wt.%) [66].

In summary, the SrBG coating on the surface of the specimens increased their hardness and stiffness. While the values of hardness for PLA/MMT and PLA/MMT/SrBG were similar, the elastic modulus of PLA/MMT/SrBG was consistently higher than the PLA/MMT. Petretta et al. [82] reported that composite scaffold of PCL/BG-Mg exhibited enhanced nanomechanical properties compared to PCL fibers. Moreover, the addition of nHA (as a second layer of coating) further enhanced the nanomechanical behavior since it is known that the hardness is related to coating thickness [83], but nHA coating on its own could not improve the stiffness of 3D printed PLA [52]. This enhanced hardness can be crucial for

biomedical applications, since better hardness can reduce the wear of an implant [84]. Corcione et al. [20] fabricated a PLA-HA composite filament for FFF with 5% HA and the flexural modulus of PLA-HA was calculated around 3000 MPa, which was a slight increase compared to pure PLA. The value of elastic modulus of PLA/MMT/SrBG/nHA can be compared with the elastic modulus of PEEK with 30% nHA and 5% MWCNT according to the study of Kumar et al. [85] (Table 4).

In vitro biomineralization

The formation of bone-like apatite on the surface of scaffolds is essential for validating their suitability in bone tissue regeneration. The in vitro bioactivity of the scaffolds was tested by incubation in SBF for 14 days and consequent examination of the surface morphology with SEM micrographs (Fig. 4, right column) and EDX spectra (Figure S3). After the incubation, spherical mineral formations were sparsely distributed on the surface of PLA and PLA/MMT scaffolds. They were identified as calcium phosphate with an atomic Ca/P ratio of 1.65, which is close to the composition of stoichiometric apatite. While distinguishing newly formed apatite structures on the PLA/MMT/SrBG and PLA/MMT/SrBG/nHA scaffolds might be difficult, it is clear that the density of the particles coated on their surfaces is much denser, and the concentration of Ca and P increased, while that of Si decreased (Figure S3 f and h). This indicates that Si was released from the bioglass, and at the same time, HA was deposited on the surface of the scaffolds. The deposits on PLA/MMT/SrBG had a Ca/P = 1.56 (calcium-deficient HA) and of PLA/MMT/SrBG/nHA Ca/P = 1.82 (calcium rich HA). Scaffolds made from glass ceramic/PLA filaments were also found able to promote biomineralization, with larger and denser apatite formations in comparison with sparse sentiments on neat PLA [86], similar to those shown in Fig. 4a. In that case thought, the mass of ceramic added in the filament was 75% that of PLA, while in the case of coatings a

significantly smaller amount of bioactive ceramic was used.

In vitro cell viability and osteogenic differentiation

The in vitro biocompatibility of the scaffolds was evaluated with MTT assay and fluorescence microscopy images, using BM-MSCs. Metabolic activity was measured after 24 and 72 h of cell seeding on the scaffolds. The results are presented in Fig. 8a. Two-way repeated measures ANOVA showed that time did not have a significant overall effect ($p > 0.05$) on cellular metabolic activity. Additionally, it was also not significantly affected by the different scaffold compositions, revealing that cell viability on the scaffolds remained satisfactory and no cytotoxicity was detected. Overall, the scaffolds did not have a negative effect on cell growth since both PLA and nHA have excellent biocompatibility and the content of Sr in SrBG is not large enough to cause cytotoxicity. The attachment of the BM-MSCs on the scaffolds after 24 h of incubation was visualized with fluorescence microscopy (Fig. 9 left column). The cells adhered and proliferated homogeneously, guided by the structures, as the whole structure have green fluorescent spots that are live cell nuclei. Upon careful examination, the cell density of neat PLA is slightly smaller in comparison with the other scaffolds. In the SEM images of Fig. 9, middle column, cells adhered and spread on the surface of the scaffold are visible. In contrast to neat PLA (Fig. 9b), the BM-MSCs cells were well embedded on the surface of the composite scaffolds (Fig. 9e, h, k), stretched and formed projections. Confirming the observations from fluorescence microscopy, fewer cells were attached to the surface of neat PLA scaffolds, since PLA is a hydrophobic polymer with known poor cell adhesion. It is, however, cytocompatible. The improved attachment and proliferation of the cells on the coated scaffolds is a result of their improved wettability and roughness.

The BM-MSCs were seeded on the scaffolds, and osteogenic differentiation was induced with a commercially available kit. After 28 d, Alizarin Red staining was performed and quantified with cetylpiridinium chloride (CPC), and the results are shown in (Fig. 8b). Since each mole of alizarine red binds to two moles of calcium, calcium deposition is proportional to CPC absorbance. The capacity of minerals deposition is a late-stage marker of osteogenic differentiation. The osteogenic potential of PLA is not significantly affected by the incorporation of MMT ($p > 0.05$). Both coatings increase the CPC absorbance, increasing thus calcium deposition, in comparison with both PLA and PLA/MMT scaffold. The two coated scaffolds PLA/MMT/SrBG and PLA/MMT/SrBG/nHA also showed increased CPC absorbance in comparison with the positive control (BM-MSCs differentiated). However, the presence of nHA did not have an important effect on CPC absorbance. These observations are a result of the intrinsic property of SrBG to induce apatite formation and favor cell differentiation and of HA to promote osteogenesis, in combination with increased surface roughness which is known to affect osteogenesis in several osteoblast-like cell models [87]. PCL scaffolds coated with bioglass and HA could improve the osteogenic differentiation of stem cells as well [88]. PLA scaffolds with 20 wt.%HA had an increased osteogenic potential and showed increased mineralization, due to the release of Ca and P ions from HA [89].

The morphology of the scaffold's surfaces after 28 d of induced differentiation toward osteocytes is shown in Fig. 9, right column. After differentiation, the cells on the PLA and PLA/MMT scaffolds have a round, osteoblast-like shape, and calcified globules were deposited. On the PLA/MMT/SrBG and PLA/MMT/SrBG/nHA scaffolds, the cells are embedded in a thick layer of deposits, with elongated shapes with cellular extensions (filopodia) bridges between the cell and the deposits, which is typical for osteoblasts [90]. Similar osteoblast-like cell morphologies were identified on the surface of HA-coated PLA scaffolds [32]. The morphology of the surface of the scaffolds PLA/MMT/SrBG and PLA/MMT/SrBG/nHA after osteogenic differentiation was examined also in higher magnifications (Fig. 10). In Fig. 10a, attached cells and mineral depositions have covered the surface. Such mineral globuli rich in Ca have been observed on substrates with bioactive glass [87]. On the surface of PLA/MMT/SrBG/nHA (Fig. 10b), wormlike apatite structures have formed, and some collagen-like fibers can be seen. More specifically, a thick layer of ECM seems to have covered parts of the surface of the PLA/MMT/SrBG/nHA scaffold, Fig. 10b.

During the osteogenic differentiation of MSCs, the organic part of the bone's ECM (called osteoid),
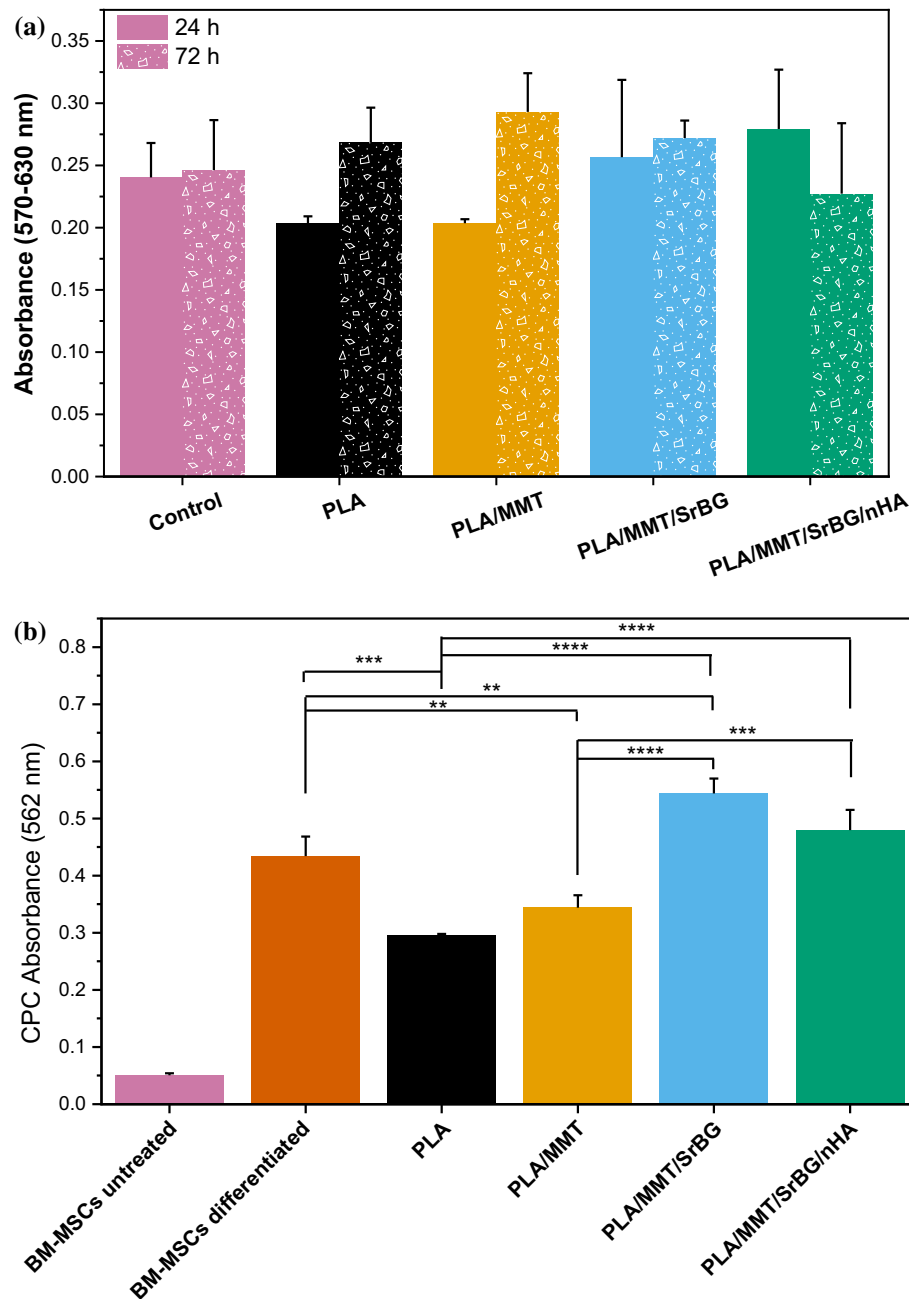
Figure 8 **a** MTT assays results and **b** assessment of osteogenic differentiation by cetylpiridinium chloride (CPC) method after 28 days in the induced differentiation culture 30 days culture on PLA, PLA/MMT, PLA/MMT/SrBG and PLA/MMT/SrBG/nHA scaffolds.$*p$ 0.01–0.05;$**p$ 0.001–0.01;$***p$ 0.0001–0.001; $****p < 0.0001$.

which is composed by 90% collagen type I, is secreted by immature osteoblasts and osteoid mineralization follows by mature osteoblasts that eventually become differentiated osteocytes [91]. The osteoid's collagen is comprised of lamellae aligned in one direction, typically $\sim$ 2 μm thick, and serves as the surface for osteoblasts to synthesize new matrix [91]. Into this organic matrix, mineral is deposited as

hydroxyapatite, during the process known as mineralization, which is a marker for the final stage of osteogenic differentiation. The increased mineralization, expressed by higher CPC levels, along with the morphological changes of the surface of the coated scaffolds in contrast to PLA and PLA/MMT suggests that the coatings were capable of promoting cell growth, proliferation and osteogenic activity.
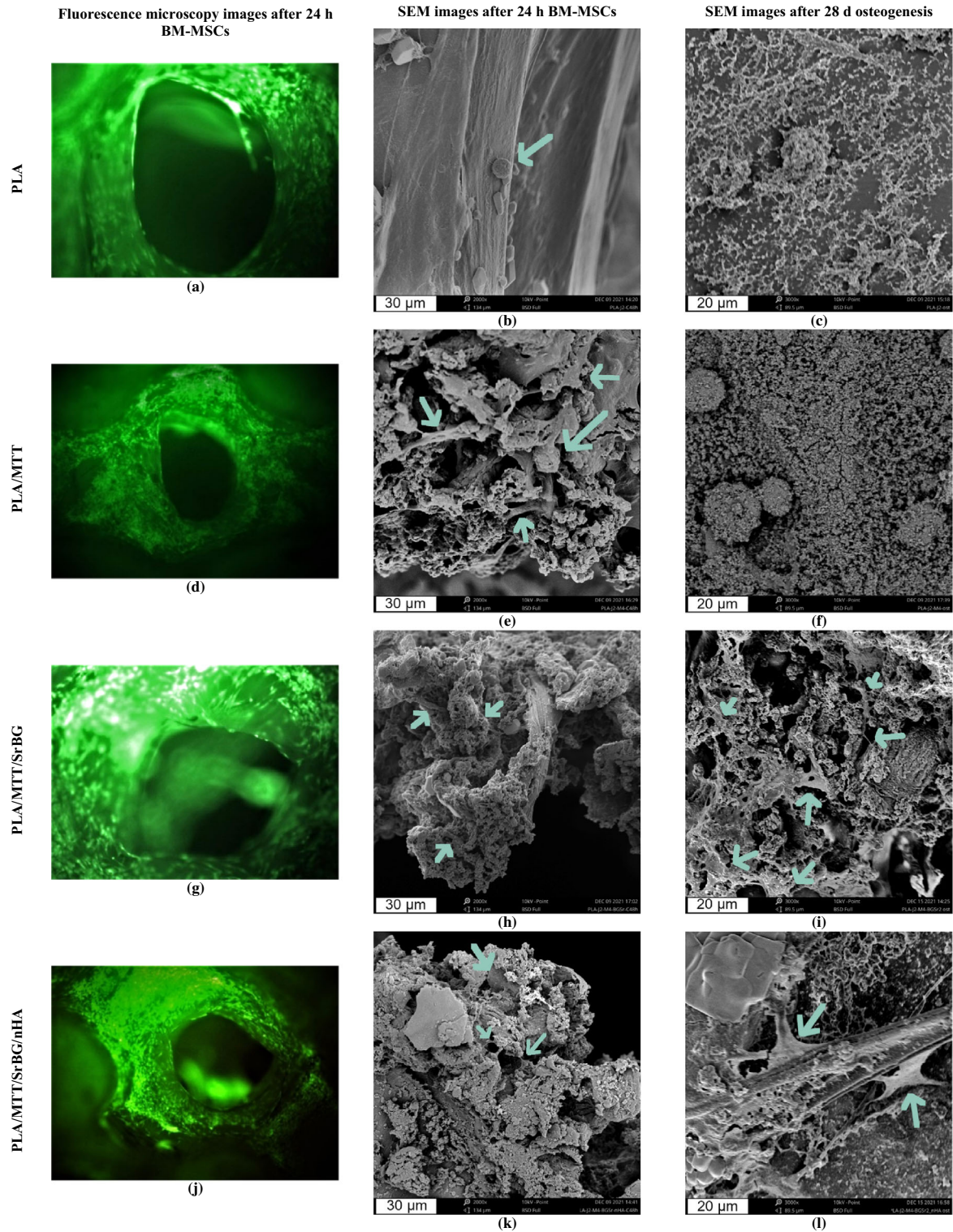
Figure 9 Fluorescence microscopy and SEM images of genetically modified BM-MSCs on the scaffolds and SEM images after 28 days of osteogenic differentiation.
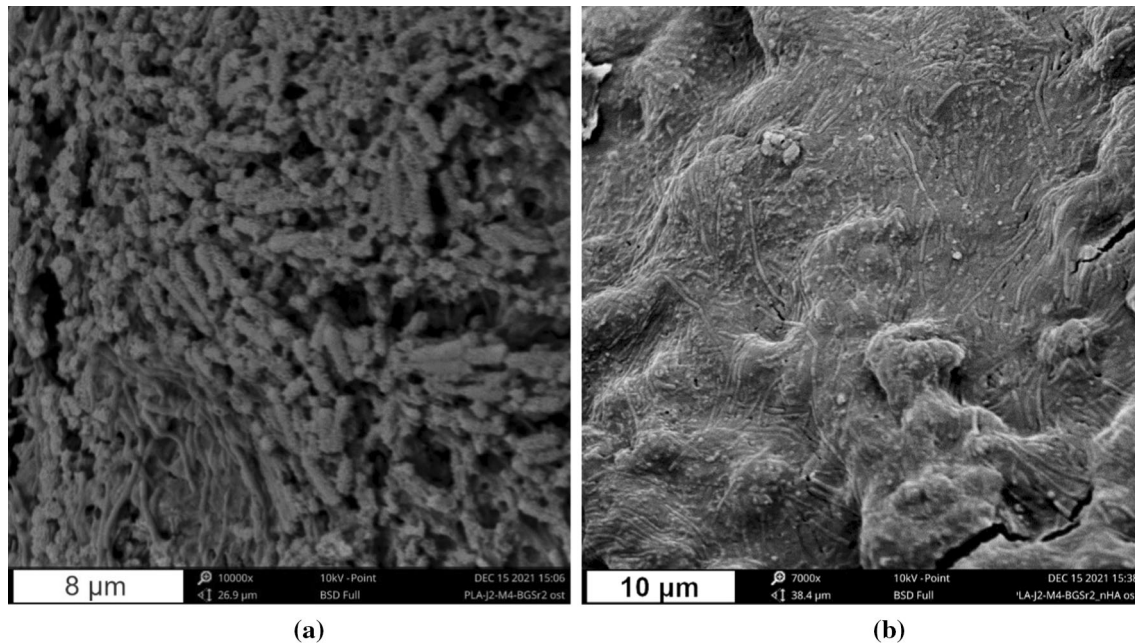
Figure 10 SEM micrographs after osteogenic differentiation showing **a** PLA/MMT/SrBG and **b** PLA/MMT/SrBG/nHA.

Conclusions

In this work, the design and manufacturing of printable PLA/MMT nanocomposite porous scaffolds using fused filament fabrication (FFF) technology were successfully demonstrated. In summary, two different types of coatings using a Sr-containing ternary ordered mesoporous bioglass as a first layer and nHA as second layer of coating on the surface of PLA/MMT 3D printed scaffolds were prepared. PLA/MMT 3D printed scaffolds with and without coating were comprehensively analyzed in terms of their physicochemical and mechanical properties, as well as through cell viability studies, which confirmed that all scaffolds have good biocompatibility and their porous designed structure create a more favorable environment for cell growth. According to the results of in vitro cell experiments and SEM analysis, the coating of scaffolds with SrBG and SrBG/nHA highly promotes cell proliferation as well as osteogenesis differentiation, confirming that the incorporation of Sr^{2+} ions induces an accelerated bioactive behavior, making them good materials for bone tissue regeneration applications. The obtained results demonstrate that coated PLA/MMT 3D printed nanocomposite scaffolds have great potential for bone scaffolds. Osteogenic differentiation can be promoted by coating the PLA/MMT 3D printed scaffolds with either SrBG or SrBG/nHA. These findings suggest SrBG and SrBG/nHA can be used as coatings instead of directly added in the bulk of polymers to improve the suitability of PLA scaffolds for bone tissue engineering applications. Such scaffolds could be used for manufacturing personalized, 3D printed orthopedic implants for animals and humans. Finally, more advanced preclinical research on the degradation of the PLA/MMT nanocomposites is required, as well as in vivo studies, in order to investigate the potential use of PLA/MMT 3D printed nanocomposite scaffolds for clinical applications.

Author's contribution

DT, DNB, MG and ZT took part in conceptualization; MG, EG and DB undertook the investigation; DT, DNB, TS and GC were responsible for resources; DT, ZT, DNB, TS and GC were involved in supervision; MG, ZT and DB wrote the original draft; and DT, ZT, KT, DNB, TS and GC participated in writing—review and editing.

Funding

Declarations

Conflict of interest The authors declare no conflict of interest.

Supplementary Information: The online version contains supplementary material available at http s://doi.org/10.1007/s10853-023-08149-4.

References

[1] Kim T, See CW, Li X, Zhu D (2020) Orthopedic implants and devices for bone fractures and defects: past. Present Perspect Eng Regen 1:6–18. https://doi.org/10.1016/j.engre g.2020.05.003

[2] Pierantozzi D, Scalzone A, Jindal S, Stīpniece L, Šalma-Ancāne K, Dalgarno K, Gentile P, Mancuso E (2020) 3D Printed Sr-containing composite scaffolds: effect of structural design and material formulation towards new strategies for bone tissue engineering. Compos Sci Technol, 191. h ttps://doi.org/10.1016/j.compscitech.2020.108069

[3] Mikael PE, Golebiowska AA, Xin X, Rowe DW, Nukavarapu SP (2020) Evaluation of an engineered hybrid matrix for bone regeneration via endochondral ossification. Ann Biomed Eng 48:992–1005. https://doi.org/10.1007/s10439-019-02279-0

[4] Jammalamadaka U, Tappa K (2018) Recent advances in biomaterials for 3D printing and tissue engineering. J Funct Biomater 9

[5] Li X, Wang L, Fan Y, Feng Q, Cui FZ, Watari F (2013) Nanostructured scaffolds for bone tissue engineering. J Biomed Mater Res A 101(A):2424–2435

[6] Babilotte J, Guduric V, le Nihouannen D, Naveau A, Fricain JC, Catros S (2019) 3D printed polymer-mineral composite biomaterials for bone tissue engineering: fabrication and characterization. J Biomed Mater Res B Appl Biomater 107:2579–2595. https://doi.org/10.1002/jbm.b.34348

[7] Qu H (2020) Additive Manufacturing for Bone Tissue Engineering Scaffolds. Mater Today Commun, 24. https://d oi.org/10.1016/j.mtcomm.2020.101024

[8] Moreno Madrid AP, Vrech SM, Sanchez MA, Rodriguez AP (2019) Advances in additive manufacturing for bone tissue engineering scaffolds. Mater Sci Eng, C 100:631–644. http s://doi.org/10.1016/j.msec.2019.03.037

[9] Nazeer MA, Onder OC, Sevgili I, Yilgor E, Kavakli IH, Yilgor I (2020) 3D printed poly(lactic acid) scaffolds modified with chitosan and hydroxyapatite for bone repair applications. Mater Today Commun 25. https://doi.org/10. 1016/j.mtcomm.2020.101515.

[10] Liu J, Mohd Rafiq NB,; Wong LM, Wang, S (2021) Surface treatment and bioinspired coating for 3D-printed implants. Front Chem, 9

[11] Mohd Pu'ad NAS, Abdul Haq RH, Mohd Noh H, Abdullah HZ, Idris MI, Lee TC (2019) Review on the fabrication of fused deposition modelling (FDM) composite filament for biomedical applications. In: Proceedings of the materials today: proceedings. Elsevier Ltd,; 29:228–232

[12] Bai T, Zhu B, Liu H, Wang Y, Song G, Liu C, Shen C (2020) Biodegradable poly(lactic acid) nanocomposites reinforced and toughened by carbon nanotubes/clay hybrids. Int J Biol Macromol 151:628–634. https://doi.org/10.1016/j.ijbiomac. 2020.02.209

[13] Terzopoulou Z, Zamboulis A, Koumentakou I, Michailidou G, Jan Noordam M, Bikiaris DN (2022) Biocompatible synthetic polymers for tissue engineering purposes.

Biomacromolecules 23:1841–1863. https://doi.org/10.1021/acs.biomac.2c00047

[14] Sahmani S, Khandan A, Esmaeili S, Saber-Samandari S, Ghadiri Nejad M, Aghdam MM (2020) Calcium phosphate-PLA scaffolds fabricated by fused deposition modeling technique for bone tissue applications: fabrication. Char Simul Ceram Int 46:2447–2456. https://doi.org/10.1016/j.ceramint.2019.09.238

[15] Chen X, Gao C, Jiang J, Wu Y, Zhu P, Chen G (2019) 3D printed porous PLA/NHA composite scaffolds with enhanced osteogenesis and osteoconductivityin vivo for bone regeneration. Biomed Mater (Bristol), 14. https://doi.org/10.1088/1748-605X/ab388d

[16] Diez-Escudero A, Harlin H, Isaksson P, Persson C (2020) porous polylactic acid scaffolds for bone regeneration: a study of additively manufactured triply periodic minimal surfaces and their osteogenic potential. J Tissue Eng, 11. https://doi.org/10.1177/2041731420956541

[17] Valiño-Cultelli V, Varela-López Ó, González-Cantalapiedra A (2021) Preliminary clinical and radiographic evaluation of a novel resorbable implant of polylactic acid (Pla) for tibial tuberosity advancement (Tta) by modified maquet technique (Mmt). Animals, 11. https://doi.org/10.3390/ani11051271

[18] Sanyang ML, Jawaid M (2019) Bio-based polymers and nanocomposites: preparation, processing, properties and performance. Springer International Publishing. ISBN 9783030058258.

[19] Tajbakhsh S, Hajiali F (2017) A comprehensive study on the fabrication and properties of biocomposites of poly(lactic acid)/ceramics for bone tissue engineering. Mater Sci Eng C 70:897–912

[20] Corcione CE, Gervaso F, Scalera F, Montagna F, Maiullaro T, Sannino A, Maffezzoli A (2017) 3D printing of hydroxyapatite polymer-based composites for bone tissue engineering. J Polym Eng 37:741–746. https://doi.org/10.1515/polyeng-2016-0194

[21] Yang WF, Long L, Wang R, Chen D, Duan S, Xu FJ (2018) Surface-modified hydroxyapatite nanoparticle-reinforced polylactides for three-dimensional printed bone tissue engineering scaffolds. J Biomed Nanotechnol 14:295–303. https://doi.org/10.1166/jbn.2018.2495

[22] Nilawar S, Uddin M, Chatterjee K (2021) Surface engineering of biodegradable implants: emerging trends in bioactive ceramic coatings and mechanical treatments. Mater Adv 2:7820–7841

[23] Chen W, Nichols L, Teer L, Clinton K, Priddy LB (2022) A hybrid coating of polydopamine and nano-hydroxyapatite enhances surface properties of 3d printed poly(lactic-co-glycolic acid) scaffolds. J Mater Sci 57:13011–13026. https://doi.org/10.1007/s10853-022-07442-y

[24] Zhang J, Tong D, Song H, Ruan R, Sun Y, Lin Y, Wang J, Hou L, Dai J, Ding J et al (2022) Osteoimmunity-regulating biomimetically hierarchical scaffold for augmented bone regeneration. Adv Mater. https://doi.org/10.1002/adma.202202044

[25] Gunputh U, Le H (2017) Composite coatings for implants and tissue engineering scaffolds. Biomed Comp, pp 111–138. https://doi.org/10.1016/B978-0-08-100752-5.00006-8

[26] Cun X, Hosta-Rigau L (2020) Topography: a biophysical approach to direct the fate of mesenchymal stem cells in tissue engineering applications. Nanomaterials 10:1–41

[27] Liu F, Xu J, Wu L, Zheng T, Han Q, Liang Y, Zhang L, Li G, Yang Y (2021) The influence of the surface topographical cues of biomaterials on nerve cells in peripheral nerve regeneration: a review. Stem Cells Int

[28] Kaniuk Ł, Krysiak ZJ, Metwally S, Stachewicz U (2020) Osteoblasts and fibroblasts attachment to poly(3-hydroxybutyric acid-co-3-hydroxyvaleric acid) (phbv) film and electrospun scaffolds. Mater Sci Eng C, 110. https://doi.org/10.1016/j.msec.2020.110668

[29] Backes EH, Fernandes EM, Diogo GS, Marques CF, Silva TH, Costa LC, Passador FR, Reis RL, Pessan LA (2021) Engineering 3D printed bioactive composite scaffolds based on the combination of aliphatic polyester and calcium phosphates for bone tissue regeneration. Mater Sci Eng C 122:111928. https://doi.org/10.1016/j.msec.2021.111928

[30] Esposito Corcione C, Gervaso F, Scalera F, Padmanabhan SK, Madaghiele M, Montagna F, Sannino A, Licciulli A, Maffezzoli A (2019) Highly loaded hydroxyapatite microsphere/ PLA porous scaffolds obtained by fused deposition modelling. Ceram Int 45:2803–2810. https://doi.org/10.1016/j.ceramint.2018.07.297

[31] Zhang B, Wang L, Song P, Pei X, Sun H, Wu L, Zhou C, Wang K, Fan Y, Zhang X (2021) 3D Printed bone tissue regenerative PLA/HA scaffolds with comprehensive performance optimizations. Mater Des, 201. https://doi.org/10.1016/j.matdes.2021.109490

[32] Mondal S, Nguyen TP, Pham VH, Hoang G, Manivasagan P, Kim MH, Nam SY, Oh J (2020) Hydroxyapatite nano bioceramics optimized 3D printed poly lactic acid scaffold for bone tissue engineering application. Ceram Int 46:3443–3455. https://doi.org/10.1016/j.ceramint.2019.10.057

[33] Prakash C, Singh G, Singh S, Linda WL, Zheng HY, Ramakrishna S, Narayan R (2021) Mechanical reliability and in vitro bioactivity of 3D-printed porous polylactic acid-hydroxyapatite scaffold. J Mater Eng Perform. https://doi.org/10.1007/s11665-021-05566-x

[34] Dubinenko G, Zinoviev A, Bolbasov E, Kozelskaya A, Shesterikov E, Novikov V, Tverdokhlebov S () Highly filled poly(l-lactic acid)/hydroxyapatite composite for 3D printing of personalized bone tissue engineering scaffolds. J Appl Polym Sci, 138. https://doi.org/10.1002/app.49662

[35] Radulescu DE, Neacsu IA, Grumezescu AM, Andronescu E (2022) Novel trends into the development of natural hydroxyapatite-based polymeric composites for bone tissue engineering. Polymers (Basel), 14

[36] Grigora M-E, Terzopoulou Z, Tsongas K, Bikiaris DN, Tzetzis D (2022) Physicochemical characterization and finite element analysis-assisted mechanical behavior of polylactic acid-montmorillonite 3D printed nanocomposites. Nanomaterials 2022, 12:2641. https://doi.org/10.3390/nano12152641

[37] Lee YH, Lee JH, An IG, Kim C, Lee DS, Lee YK, Nam J (2005) Do electrospun dual-porosity structure and biodegradation morphology of montmorillonite reinforced PLLA nanocomposite scaffolds. Biomaterials 26:3165–3172. https://doi.org/10.1016/j.biomaterials.2004.08.018

[38] Lee JH, Park TG, Park HS, Lee DS, Lee YK, Yoon SC, Nam J (2003) Do thermal and mechanical characteristics of poly(l-lactic acid) nanocomposite scaffold. Biomaterials 24:2773–2778. https://doi.org/10.1016/S0142-9612(03)00080-2

[39] Koç Demir A, Elçin AE, Elçin YM (2018) Strontium-modified chitosan/montmorillonite composites as bone tissue engineering scaffold. Mater Sci Eng, C 89:8–14. https://doi.org/10.1016/j.msec.2018.03.021

[40] Olad A, Farshi Azhar F (2014) The synergetic effect of bioactive ceramic and nanoclay on the properties of chitosan-gelatin/nanohydroxyapatite-montmorillonite scaffold for bone tissue engineering. Ceram Int 40:10061–10072. https://doi.org/10.1016/j.ceramint.2014.04.010

[41] Fredholm YC, Karpukhina N, Brauer DS, Jones JR, Law RV, Hill RG (2012) Influence of strontium for calcium substitution in bioactive glasses on degradation, ion release and apatite formation. J R Soc Interface 9:880–889. https://doi.org/10.1098/rsif.2011.0387

[42] Ningsih HS, Liu YC, Chen JW, Chou YJ (2022) Effects of strontium dopants on the in vitro bioactivity and cytotoxicity of strontium-doped spray-dried bioactive glass microspheres. J Non Cryst Solids, 576. https://doi.org/10.1016/j.jnoncrysol.2021.121284

[43] Terzopoulou Z, Baciu D, Gounari E, Steriotis T, Charalambopoulou G, Tzetzis D, Bikiaris D (2019) composite membranes of poly(ε-caprolactone) with bisphosphonate-loaded bioactive glasses for potential bone tissue engineering applications. Molecules, 24. https://doi.org/10.3390/molecules24173067

[44] Alksne M, Kalvaityte M, Simoliunas E, Rinkunaite I, Gendviliene I, Locs J, Rutkunas V, Bukelskiene V (2020) In vitro comparison of 3D printed polylactic acid/hydroxyapatite and polylactic acid/bioglass composite scaffolds: insights into materials for bone regeneration. J Mech Behav Biomed Mater, 104. https://doi.org/10.1016/j.jmbbm.2020.103641

[45] Oryan A, Eslaminejad MB, Kamali A, Hosseini S, Sayahpour FA, Baharvand H (2018) Synergistic effect of strontium. Bioactive Glass Nano Hydroxyapatite Promotes Bone Regeneration Critical Sized Radial Bone Defects. https://doi.org/10.1002/jbm.b.34094

[46] Baciu D (2015) Synthesis and characterization of well-ordered mesoporous bioglass nanospheres for biomedical applications. In: National Hellenic Research Foundation, (ed), Proceedings of the 10th anniversary conference of the hellenic society for biomaterials: Athens, 26 Nov 2015

[47] Karageorgiou V, Kaplan D (2005) Porosity of 3D biomaterial scaffolds and osteogenesis. Biomaterials 26:5474–5491

[48] van Bael S, Chai YC, Truscello S, Moesen M, Kerckhofs G, van Oosterwyck H, Kruth JP, Schrooten J (2012) The effect of pore geometry on the in vitro biological behavior of human periosteum-derived cells seeded on selective laser-melted Ti6Al4V bone scaffolds. Acta Biomater 8:2824–2834. https://doi.org/10.1016/j.actbio.2012.04.001

[49] Tang X, Qin Y, Xu X, Guo D, Ye W, Wu W, Li R (2019) Fabrication and in vitro evaluation of 3D printed porous polyetherimide scaffolds for bone tissue engineering. Biomed Res Int. https://doi.org/10.1155/2019/2076138

[50] Abbasi N, Hamlet S, Love RM, Nguyen NT (2020) Porous scaffolds for bone regeneration. J Sci Adv Mater Devices 5:1–9

[51] Grigora ME, Terzopoulou Z, Tsongas K, Klonos P, Kalafatakis N, Bikiaris DN, Kyritsis A, Tzetzis D (2021) Influence of reactive chain extension on the properties of 3D printed poly(lactic acid) constructs. Polymers (Basel), 13. https://doi.org/10.3390/polym13091381

[52] Chen W, Nichols L, Brinkley F, Bohna K, Tian W, Priddy MW, Priddy LB (2021) Alkali treatment facilitates functional nano-hydroxyapatite coating of 3D printed polylactic acid scaffolds. Mater Sci Eng C, 120. https://doi.org/10.1016/j.msec.2020.111686

[53] Kokubo T, Takadama H (2006) How useful is sbf in predicting in vivo bone bioactivity? Biomaterials 27:2907–2915. https://doi.org/10.1016/j.biomaterials.2006.01.017

[54] Gounari E, Daniilidis A, Tsagias N, Michopoulou ANNA, Kouzi K, Koliakos G (2019) Isolation of a novel embryonic stem cell cord blood–derived population with in vitro hematopoietic capacity in the presence of Wharton's Jelly–

derived mesenchymal stromal cells. Cytotherapy 21:246–259. https://doi.org/10.1016/j.jcyt.2018.11.006

[55] Koliakou I, Gounari E, Nerantzaki M, Pavlidou E, Bikiaris D, Kaloyianni M, Koliakos G (2019) Differentiation capacity of monocyte-derived multipotential cells on nanocomposite poly(e-caprolactone)-based thin films. Tissue Eng Regen Med 16:161–175. https://doi.org/10.1007/s13770-019-00185-z

[56] Terzopoulou Z, Baciu D, Gounari E, Steriotis T, Charalambopoulou G, Bikiaris D (2018) Biocompatible nanobioglass reinforced poly(ε-caprolactone) composites synthesized via in situ ring opening polymerization. Polymers (Basel), 10. https://doi.org/10.3390/polym10040381

[57] Fujikura K, Karpukhina N, Kasuga T, Brauer DS, Hill RG, Law RV (2012) Influence of strontium substitution on structure and crystallisation of bioglass® 45S5. J Mater Chem 22:7395–7402. https://doi.org/10.1039/c2jm14674f

[58] Taherkhani S, Moztarzadeh F (2016) Influence of strontium on the structure and biological properties of sol–gel-derived mesoporous bioactive glass (MBG) powder. J Solgel Sci Technol 78:539–549. https://doi.org/10.1007/s10971-016-3995-2

[59] Shahrabi S, Hesaraki S, Moemeni S, Khorami M (2011) structural discrepancies and in vitro nanoapatite formation ability of sol-gel derived glasses doped with different bone stimulator ions. Ceram Int 37:2737–2746. https://doi.org/10.1016/j.ceramint.2011.04.025

[60] Moghanian A, Nasiripour S, Koohfar A, Sajjadnejad M, Hosseini SM, Taherkhani M, Miri Z, Hosseini SH, Aminitabar M, Rashvand A (2021) Characterization, in vitro bioactivity and biological studies of sol-gel-derived TiO2 substituted 58S bioactive glass. Int J Appl Ceram Technol 18:1430–1441. https://doi.org/10.1111/ijac.13782

[61] Luz GM, Mano JF (2011) Preparation and characterization of bioactive glass nanoparticles prepared by sol-gel for biomedical applications. Nanotechnology, 22. https://doi.org/10.1088/0957-4484/22/49/494014

[62] Wang X, Zhang Y, Ma Y, Chen D, Yang H, Li M (2016) Selenium—containing mesoporous bioactive glass particles: physicochemical and drug delivery properties. Ceram Int 42:3609–3617. https://doi.org/10.1016/j.ceramint.2015.11.024

[63] Hsu FY, Weng RC, Lin HM, Lin YH, Lu MR, Yu JL, Hsu HW (2015) A biomimetic extracellular matrix composed of mesoporous bioactive glass as a bone graft material. Microporous Mesoporous Mater 212:56–65. https://doi.org/10.1016/j.micromeso.2015.03.027

[64] Szymczyk-Ziółkowska P, Łabowska MB, Detyna J, Michalak I, Gruber P (2020) A review of fabrication polymer scaffolds for biomedical applications using additive

manufacturing techniques. Biocybern Biomed Eng 40:624–638. https://doi.org/10.1016/j.bbe.2020.01.015

[65] Fathi A, Kermani F, Behnamghader A, Banijamali S, Mozafari M, Baino F, Kargozar S (2021) Three-dimensionally printed polycaprolactone/multicomponent bioactive glass scaffolds for potential application in bone tissue engineering. Biomedical Glasses 6:57–69. https://doi.org/10.1515/bglass-2020-0006

[66] Distler T, Fournier N, Grünewald A, Polley C, Seitz H, Detsch R, Boccaccini, AR (2020) Polymer-bioactive glass composite filaments for 3D scaffold manufacturing by fused deposition modeling: fabrication and characterization. Front Bioeng Biotechnol, 8. https://doi.org/10.3389/fbioe.2020.00552

[67] Sztorch B, Brząkalski D, Pakuła D, Frydrych M, Špitalský Z, Przekop RE (2022) Natural and synthetic polymer fillers for applications in 3D printing—FDM technology area. Solids 3:508–548. https://doi.org/10.3390/solids3030034

[68] Rajakaruna RADNV, Subeshan B, Asmatulu E (2022) Fabrication of hydrophobic PLA filaments for additive manufacturing. J Mater Sci 57:8987–9001. https://doi.org/10.1007/s10853-022-07217-5

[69] Schätzlein E, Kicker C, Söhling N, Ritz U, Neijhoft J, Henrich D, Frank J, Marzi I, Blaeser A (2022) 3D-printed PLA-bioglass scaffolds with controllable calcium release and MSC adhesion for bone tissue engineering. Polymers (Basel), 14. https://doi.org/10.3390/polym14122389

[70] Alksne M, Kalvaityte M, Simoliunas E, Rinkunaite I, Gendviliene I, Locs J, Rutkunas V, Bukelskiene V(2020) In vitro comparison of 3D printed polylactic acid/hydroxyapatite and polylactic acid/bioglass composite scaffolds: insights into materials for bone regeneration. J Mech Behav Biomed Mater 104:10364,. https://doi.org/10.1016/J.JMBBM.2020.103641

[71] Wang C, Meng C, Zhang Z, Zhu Q (2022) 3D printing of polycaprolactone/bioactive glass composite scaffolds for in situ bone repair. Ceram Int 48:7491–7499. https://doi.org/10.1016/J.CERAMINT.2021.11.293

[72] Larrañaga A, Sarasua JR (2013) Effect of bioactive glass particles on the thermal degradation behaviour of medical polyesters. Polym Degrad Stab 98:751–758. https://doi.org/10.1016/j.polymdegradstab.2012.12.015

[73] Blaker JJ, Bismarck A, Boccaccini AR, Young AM, Nazhat SN (2010) Premature degradation of poly(α-hydroxyesters) during thermal processing of bioglass®-containing composites. Acta Biomater 6:756–762. https://doi.org/10.1016/j.actbio.2009.08.020

[74] Puppi D, Chiellini F, Piras AM, Chiellini E (2010) Polymeric materials for bone and cartilage repair. Progress in Polymer Science (Oxford) 35:403–440

[75] Liu C, Chan KW, Shen J, Liao CZ, Yeung KWK, Tjong SC (2016) Polyetheretherketone hybrid composites with bioactive nanohydroxyapatite and multiwalled carbon nanotube fillers. Polymers (Basel), 8. https://doi.org/10.3390/polym8120425

[76] Sattary M, Rafienia M, Kazemi M, Salehi H, Mahmoudzadeh M (2019) Promoting effect of nano hydroxyapatite and vitamin D3 on the osteogenic differentiation of human adipose-derived stem cells in polycaprolactone/gelatin scaffold for bone tissue engineering. Mater Sci Eng, C 97:141–155. https://doi.org/10.1016/j.msec.2018.12.030

[77] Pharr GM (1992) An improved technique for determining hardness and elastic modulus using load and displacement sensing indentation experiments. J Mater Res 7:1564–1583. https://doi.org/10.1557/JMR.1992.1564

[78] Mansour G, Zoumaki M, Tsongas K, Tzetzis D (2021) Microstructural and finite element analysis—assisted nanomechanical characterization of maize starch nanocomposite films. Mater Res, 24. https://doi.org/10.1590/1980-5373-MR-2020-0409

[79] Kourtidou D, Tsongas K, Grigora ME, Tzetzis D, Bikiaris DN, Chrissafis K (2021) On the improved mechanical properties of ball-milled gnps reinforced short chain branched-polyethylene nanocomposite: micromechanical modeling and fractography study. Appl Sci (Switzerland), 11. https://doi.org/10.3390/app11209420

[80] Tsongas K, Tzetzis D, Karantzalis A, Banias G, Exarchos D, Ahmadkhaniha D, Zanella C, Matikas T, Bochtis D (2019) Microstructural, surface topology and nanomechanical characterization of electrodeposited Ni-P/SiC nanocomposite coatings. Appl Sci (Switzerland), 9. https://doi.org/10.3390/app9142901

[81] Kourtidou D, Grigora M-E, Tzetzis D, Bikiaris DN, Chrissafis K (2022) Graphene nanoplatelets' effect on the crystallization, glass transition, and nanomechanical behavior of poly(ethylene 2,5-furandicarboxylate) nanocomposites. Molecules 27:6653. https://doi.org/10.3390/molecules27196653

[82] Petretta M, Gambardella A, Boi M, Berni M, Cavallo C, Marchiori G, Maltarello MC, Bellucci D, Fini M, Baldini N et al. (2021) Composite scaffolds for bone tissue regeneration based on Pcl and Mg-containing bioactive glasses. Biology (Basel), 10. https://doi.org/10.3390/biology10050398

[83] Graphite Coatings for Biomedical Implants_ A Focus on Anti-Thrombosis and Corrosion Resistance Properties _ Elsevier Enhanced Reader.

[84] Saini M (2015) Implant biomaterials: a comprehensive review. World J Clin Cases 3:52. https://doi.org/10.12998/wjcc.v3.i1.52

[85] Kumar M, Kumar R, Kumar S (2021) Synergistic effect of carbon nanotubes and nano-hydroxyapatite on mechanical properties of polyetheretherketone based hybrid nanocomposites. Polym Polym Compos 29:1365–1376. https://doi.org/10.1177/0967391120969503

[86] Saberi A, Behnamghader A, Aghabarari B, Yousefi A, Majda D, Huerta MVM, Mozafari M (2022) 3D direct printing of composite bone scaffolds containing polylactic acid and spray dried mesoporous bioactive glass-ceramic microparticles. Int J Biol Macromol 207:9–22. https://doi.org/10.1016/J.IJBIOMAC.2022.02.067

[87] Dieudonn SC, van den Dolder J, de Ruijter JE, Paldan H, Peltola T, van 't Hof MA, Happonen RP, Jansen JA. (2002) Osteoblast differentiation of bone marrow stromal cells cultured on silica gel and sol-gel-derived titania, 23

[88] Fazeli N, Arefian E, Irani S, Ardeshirylajimi A, Seyedjafari E (2021) 3D-printed PCL scaffolds coated with nanobioceramics enhance osteogenic differentiation of stem cells. ACS Omega 6:35284–35296. https://doi.org/10.1021/acsomega.1c04015

[89] Bernardo MP, da Silva BCR, Hamouda AEI, de Toledo MAS, Schalla C, Rütten, S, Goetzke, R, Mattoso LHC, Zenke M, Sechi A (2022) PLA/hydroxyapatite scaffolds exhibit in vitro immunological inertness and promote robust osteogenic differentiation of human mesenchymal stem cells without osteogenic stimuli. Sci Rep, 12. https://doi.org/10.1038/s41598-022-05207-w

[90] Wang YW, Wu Q, Chen GQ (2004) Attachment, Proliferation and Differentiation of Osteoblasts on Random Biopolyester Poly(3-Hydroxybutyrate-Co-3-Hydroxyhexanoate) Scaffolds. Biomaterials 25:669–675. https://doi.org/10.1016/S0142-9612(03)00561-1

[91] Lin X, Patil S, Gao YG, Qian A (2020) The bone extracellular matrix in bone formation and regeneration. Front Pharmacol, 11

Springer